Title: Agrin induces long term osteochondral regeneration by supporting repair morphogenesis

Single Sentence Summary: Agrin recruits joint stem cells and induces the formation of cartilage and bone to heal joint surface defects in mice and sheep.

Authors: Suzanne E. Eldridge[1]*, Aida Barawi[1], Hui Wang[2], Anke J. Roelofs[2], Magdalena Kaneva[1], Zeyu Guan[1], Helen Lydon[3], Bethan L. Thomas[4], Anne-Sophie Thorup[1], Beatriz F. Fernandez[1], Sara Caxaria[1], Danielle Strachan[1], Ahmed Ali[1], Kanatheepan Shanmuganathan[1], Costantino Pitzalis[1], James R. Whiteford[5], Frances Henson[6], Andrew W. McCaskie[3], Cosimo De Bari[2] and Francesco Dell'Accio[1]*.

* Corresponding author. Email: suzanne.e.eldridge@gmail.com (S.E.E.), fdellaccio@gmail.com (F.D.)

Affiliations:

[1]Centre for Experimental Medicine and Rheumatology, William Harvey Research Institute, Barts and the London School of Medicine and Dentistry, Queen Mary University of London, London, UK, EC1M 6BQ.

[2]Arthritis & Regenerative Medicine Laboratory, Aberdeen Centre for Arthritis and Musculoskeletal Health, University of Aberdeen, Aberdeen, UK, AB25 2ZD.

[3]Division of Trauma & Orthopaedic Surgery, Department of Surgery, University of Cambridge, Addenbrooke's Hospital, Cambridge, UK, CB2 2QQ.

[4]Centre for Biochemical Pharmacology, William Harvey Research Institute, Barts and the London School of Medicine and Dentistry, Queen Mary University of London, London, UK, EC1M 6BQ.

[5]Comparative Musculoskeletal Biology Group, Department of Veterinary Medicine, University of Cambridge, Madingley Road, Cambridge, UK, CB3 0ES.

[6]Centre for Microvascular Research, William Harvey Research Institute, Barts and the London School of Medicine and Dentistry, Queen Mary University of London, London, UK, EC1M 6BQ.

Abstract: Cartilage loss leads to osteoarthritis, the most common cause of disability for which there is no cure. Cartilage regeneration, therefore, is a priority in medicine. We report that agrin is a potent chondrogenic factor and that a single intra-articular administration of agrin induced long-lasting regeneration of critical-size osteochondral defects in mice, with restoration of tissue architecture and bone-cartilage interface. Agrin attracted joint resident progenitor cells to the site of injury and, through simultaneous activation of CREB and suppression of canonical WNT signaling downstream of β-catenin, induced expression of the chondrogenic stem cell marker GDF5 and differentiation into stable articular chondrocytes, forming stable articular cartilage. In sheep, an agrin-containing collagen gel resulted in long-lasting regeneration of bone and cartilage, which promoted increased ambulatory activity. Our findings support the therapeutic use of agrin for joint surface regeneration.

Introduction

Articular cartilage overlies subchondral bone at the joint surface and enables the frictionless movement of joints. Whereas bone has a high turnover and heals well, cartilage is avascular, has a low turnover, and often fails to repair after injury *(1)*. This results in further cartilage loss and osteoarthritis, the most common form of arthritis, which causes pain and disability. Currently, there is no pharmacological therapy to restore cartilage or slow cartilage loss. Osteoarthritis is therefore, along with cardiovascular disease, the leading cause of chronic disability, costing around 1.5-2% of the gross domestic product (GDP) for westernized countries *(2)*.

Joint surface defects are common*(3, 4)* and, when exceeding a critical size, heal poorly. When successful, the repair of small osteochondral defects involves trafficking of specialized mesenchymal stem cells (MSCs) ontogenetically derived from the growth differentiation factor 5 (GDF5)-expressing cells of the embryonic joint interzone to the injury site *(5, 6)*. During embryonic development, MSCs are recruited from SOX9-expressing progenitor cells, transiently express GDF5, and give rise to the articular cartilage, menisci, and ligaments *(7)*. In adulthood, GDF5-lineage progenitor cells persist in the synovial membrane (SM-MSCs) *(5, 6)*. At the bottom of the defect, the repair cartilage is invaded by vessels and replaced by bone through endochondral bone formation, which proceeds towards the surface of the defect and stops at the level of the osteochondral junction *(8–10)*. The most superficial layer of cartilage remains avascular and is resistant to endochondral bone formation *(8, 9)*. Although this morphogenetic process takes place over several weeks in rodents and several months in humans, at the molecular level, the mesenchyme becomes patterned long before morphological changes become obvious *(10)*. Such

patterning displays striking similarity to that of developing joints during embryonic morphogenesis.

During skeletal development, the chondrogenic mesenchyme forming the skeletal templates becomes segmented by the joint interzones, where specific molecular markers — including WNT9A and GDF5, a member of the bone morphogenetic protein (BMP) family of morphogens — indicate the location where joints will form *(6, 11–13)*. Through the process of cavitation, a fissure forms in the center of the joint interzones, eventually separating the skeletal elements. Meanwhile, the center of the cartilaginous template undergoes vascular invasion and chondrocytes undergo hypertrophy (expressing markers such as COL10A1) and are eventually replaced by bone. In the long bones, this process starts at the center (diaphysis) and proceeds towards the growth plate. Secondary ossification centers then form near the joints, in the epiphysis, to form the subchondral spongiosa containing bone marrow. The last few layers of chondrocytes closest to the joint cavity are spared from undergoing endochondral bone formation and form the articular cartilage. Lineage tracking experiments have established that the cells that form the articular cartilage (which persists throughout life), and those of the epiphyseal cartilage (destined to be replaced by bone), derive from distinct lineages, the former expressing GDF5 during embryonic joint formation *(7, 12, 14)*.

Members of the WNT family of morphogens (WNT4, WNT9A, and WNT16) are the earliest markers of the joint interzone *(11, 15)*. The activation of the WNT pathway is both required *(11, 15)* and sufficient to initiate the process of joint morphogenesis *(15)*. The ectopic expression of Wnt9a was shown to trigger the ectopic expression of other joint interzone markers including *Gdf5* *(11)*. During development, WNT signaling prevents the premature differentiation of the joint

interzone cells into mature chondrocytes. In adulthood, WNT signaling maintains a population of chondroprogenitors at the surface of the cartilage by preventing their differentiation into mature chondrocytes *(12, 16)*. Due to its anti-chondrogenic effect however, excessive activation of WNT signaling within the joint predisposes to osteoarthritis *(17, 18)*.

WNTs are secreted signaling molecules involved in the regulation of cell proliferation, polarity, morphogenesis and differentiation *(19)* during both development and adulthood. In the absence of WNTs, the intracellular protein β-catenin is constitutively phosphorylated by GSK-3β and is degraded through the proteasome pathway. In the presence of so called "canonical" WNTs such as WNT1, WNT3A, or WNT8, the heterodimerization of frizzled (FZD) receptors and their co-receptors LRP5 and 6 results in de-activation of GSK-3β and consequent stabilization of β-catenin. Stabilized β-catenin is transported to the nucleus where it interacts with the transcription factors TCF/LEF and activates transcription of target genes *(19)*. Other WNT ligands, such as WNT5A, activate other calcium-dependent pathways, collectively denominated "non-canonical". One of these non-canonical pathways is mediated by the intracellular kinase CaMKII and the transcription factor CREB*(20)*. In many cells, including articular chondrocytes, activation of the non-canonical WNT signaling results in inhibition of the canonical pathway *(21)*.

In this study we report that AGRIN , a signaling proteoglycan (encoded by the gene *AGRN*) best known for its role at the neuromuscular junction, where it stabilizes the clustering of the acetylcholine receptors *(22)* by binding to its receptor LRP4 *(23)*, is an orchestrator of repair morphogenesis at the joint surface by modulating multiple signaling pathways. Agrin is composed of a large N-terminal portion that binds to components of the basal membrane and a biologically active C-terminal portion encompassing three globular domains separated by EGF-like repeats

(24). Agrin is expressed in a splice isoform devoid of the y and z motifs, playing a role not only in differentiation of mature articular chondrocytes *(25)* but also in chondrogenesis and in the repair of osteochondral defects.

Results

AGRIN is upregulated in injured cartilage and induces chondrogenesis in MSCs

In the context of screening for genes upregulated after acute cartilage injury *(26)*, we discovered that agrin was upregulated at the mRNA and protein level twenty-four hours after mechanical injury to human articular cartilage explants ex vivo (Fig. 1, A to C). *AGRN* mRNA was also upregulated in C28/I2 human chondrocytes by treatment with IL-1β (Fig. 1D) and TNF-α (Fig. 1E), two inflammatory cytokines released by injured cartilage *(26–29)*. Agrin upregulation in adult primary human articular chondrocytes after IL-1β treatment was confirmed as assessed by mining a publicly accessible gene expression dataset *(30)* (fig. S1A). Compared to green fluorescent protein (GFP), used hereafter as transfection control, agrin overexpression in human adult synovial membrane-derived mesenchymal stem cells (SM-MSCs) *(5, 31)* resulted in their differentiation into cartilage as assessed by increased production of cartilage-specific Alcian blue-positive extracellular matrix and upregulation of the cartilage master transcription factor *SOX9* mRNA (Fig. 1, F and G). Together, these data show that agrin is upregulated in injured cartilage and induces chondrogenic differentiation in SM-MSCs that normally reside in the joint.

Agrin induces chondrogenesis by suppressing WNT signaling downstream of β-catenin

Next, we investigated the molecular pathway underlying the chondrogenic effect of agrin. The agrin receptor LDL receptor related protein 4 (LRP4) mediates chondrocytic differentiation in the murine chondrocytic cell line ATDC5 by inhibiting canonical WNT signaling *(32)*. We found that overexpression of either LRP4 (Fig. 2A) or agrinitself (Fig. 2B), both in the absence and presence of WNT3A, in primary bovine chondrocytes upregulated *SOX9* mRNA. LRP4 is known to bind to and mediate the function of WNT inhibitory molecules such as DKK1 and SOST *(33)*; therefore, we investigated whether agrinis required for the chondrogenic function of LRP4. Silencing *AGRN* in C28I/2 chondrocytes prevented the *SOX9* upregulation induced by LRP4 overexpression (Fig. 2C). These data indicate that agrin is necessary for the chondrogenic effects of LRP4. Agrin silencing did not alter expression of *DKK1* mRNA (fig. S1B). *SOST* is not expressed in articular chondrocytes and was not detected by PCR.

Canonical WNT signaling is known to suppress chondrogenesis *(12, 16)*. Agrin overexpression blocked the capacity of WNT3A and WNT9A to activate the WNT/β-catenin-dependent reporter assay TOPFlash *(34)* (Fig. 2, D and E). Overexpression of either LRP4 or agrin suppressed TOPFlash activation in a WNT3A dose-response curve and co-overexpression of LRP4 and agrin was synergisticfurther inhibited TOPFlash activation (Fig. 2F). Moreover, agrin failed to induce extracellular matrix formation in C28/I2 chondrocytes in which activation of canonical WNT signaling was achieved directly in the nucleus by overexpressing a constitutively active form of LEF1 (caLEF1) composed of the transactivation domain of VP16 and the DNA-binding domain of LEF1 *(35)* (Fig. 2G). Therefore, the capacity of agrin to suppress canonical WNT signaling is

essential to its chondrogenic effect. Taken together, these data indicate that agrin induces chondrogenesis by suppressing canonical WNT signaling.

To test at what level in the signaling cascade agrininhibits WNTs, we activated WNT signaling in COS7 cells using either the GSK-3β inhibitor BIO *(36)* or the inhibitor of AXIN/GSK3-β interaction SKL2001 *(37)*. Disruption of the β-catenin destruction complex with either compound resulted in ligand/receptor-independent activation of the TOPFlash reporter assay; however, agrin overexpression was still able to inhibit such activation (Fig 3, A and B), thereby demonstrating that the capacity of agrin to inhibit canonical WNT signaling resides downstream of the β-catenin destruction complex. Similarly, agrin inhibited the activation of the TOPFlash reporter assay induced by overexpression of constitutively active β-catenin [CTNNB1(Δex3), caCTNNB1] *(38)* (Fig 3C). In keeping with the notion that agrin acts downstream of the β-CATENIN destruction complex, agrin enhanced extracellular matrix production in C28/I2 chondrocytes even in the presence of SKL2001 (fig. S2). However, when COS7 cells were transfected with caLEF1, Agrin was unable to prevent activation of the TOPFlash reporter (Fig.3D). Taken together, these data suggest that agrin suppresses canonical WNT signaling downstream of β-catenin.

Agrin activates CREB signaling

Agrin was previously reported to activate the Calcium/CaMKII/CREB signaling pathway in neurons *(39–41)*. We therefore hypothesized that agrin might be blocking canonical WNT signaling downstream of β-catenin by activating the CaMKII/CREB pathway *(21)*. Agrin transfection or exogenous recombinant agrin resulted in phosphorylation and consequent

activation of CREB (pCREB) in C28/I2 chondrocytes (Fig. 3, E to H and fig. S3) and activation of a CREB reporter assay *(42)* (Fig 3I). Conversely, silencing endogenous *AGRN* in C28/I2 cells using siRNA resulted in a decrease in the number of phosphorylated CREB-positive cells, while total CREB-positive cells remained unchanged (Fig. 3, J to L).

In the presence of the CREB inhibitor 666-15 *(43)*, agrin failed to suppress the capacity of WNT3A to activate the TOPFlash reporter assay (Fig 4A), suggesting that the capacity of agrin to inhibit WNT signaling is mediated by CREB. Confirming the epistasis of CaMKII in the CREB activation cascade *(39, 40)*, the CaMKII inhibitors KN93 and AIP negated the capacity of agrin to suppress the activation of the TOPFlash reporter assay induced by WNT3A when compared to KN92 (inactive control) or vehicle control respectively (Fig. 4B andC). Several signaling pathways converge onto the CREB pathway with distinct, context-dependent transcriptional and biological outcomes *(44–47)*. Therefore, we investigated whether the capacity to suppress canonical WNT signaling is specific to agrin or is a general effect of CREB activation. Forskolin, an activator of adenyl cyclase and CREB agonist, failed to inhibit activation of the TOPFlash reporter assay after WNT3A treatment (Fig. 4D). Therefore, CREB activation is required but not *per se* sufficient for the capacity of agrin to suppress WNT signaling. We next tested whether agrin-induced CREB activation is essential for its chondrogenic capacity. In keeping with this hypothesis, agrin or LRP4 lost the capacity to enhance extracellular matrix formation in C28I/2 chondrocytes in the presence of the CREB inhibitor 666-15 (Fig. 4E to H). Taken together, these data demonstrate that agrin activates the CaMKII/CREB cascade and that these events are essential for its capacity to inhibit WNT signaling and to induce cartilage formation.

Agrin supports the repair of critical size osteochondral joint surface defects in mice.

To test if exogenous agrin is sufficient to improve the outcome of joint surface repair *in vivo*, we generated cylindrical osteochondral defects in the lateral femoral condyle of adult mice. Defects were 0.78±0.042 mm wide and 1.79±0.056 mm deep (mean±SD) and extended into the subchondral spongiosa. Without treatment, such defects result in partial healing of the bone, but not of the articular cartilage or the subchondral plate, after 8 weeks (fig. S4A-B). A type I collagen gel containing either human full-length agrin or GFP as control was injected into the joint surface defect immediately after it was generated. Eight weeks after surgery, the cartilage layer regenerated significantly better in the agrin group (Fig. 5A) both in terms of glycosaminoglycan content *(48)* (P=0.04141) (Fig. 5B) and Pineda injury score *(49)* (P=0.04083) (Fig. 5C). The size of the residual bone defect was also reduced in the agrin group (Fig. 5D), however no evidence of ectopic bone formation was observed by µCT (fig. S4C). Whereas in the agrin group most of the repair tissue was composed of either bone or cartilage, in the GFP group there was a larger amount of non-differentiated fibroblast-like mesenchyme (Fig. 5E).

Agrin induces GDF5 upregulation in a CREB-dependent manner

We previously reported that the cells that contribute to the repair of cartilage defects derive from a lineage of progenitor cells that, during skeletal development, express the joint interzone marker GDF5 *(5)*. During skeletal development, WNT9A induces the expression of GDF5 in the mesenchymal cells residing in the portion of the skeletal elements that will give rise to the articular cartilage, menisci, and ligaments, and that are resistant to endochondral bone formation *(7, 11,*

13). In adulthood, joint-specific progenitor cells derived from the GDF5 lineage persist within the synovial membrane and are the main contributors to the regeneration of cartilage defects, which, when small in size, repair spontaneously *(5, 9)*. Unstimulated human SM-MSCs did not express detectable GDF5, however, 24 hr after agrin transfection, many of the cells highly expressed GDF5 (Fig. 6A). In addition, agrin transfection induced GDF5 upregulation in C28/I2 human chondrocytes at protein (Fig. 6B-C) and mRNA levels (Fig. 6D). Conversely, silencing of endogenous *AGRN* using siRNA in C28/I2 cells resulted in a reduction of GDF5 expression at protein (Fig. 6 E and F) and mRNA levels (Fig. 6G). This loss of GDF5 was rescued with the addition of exogenous rAgrin (Fig. 6E and F). Strikingly, agrin was unable to induce GDF5 expression in bone marrow-derived MSCs (fig. S5). This suggests that the capacity of agrin to induce GDF5 is restricted to cells of the GDF5-derived lineage, such as chondrocytes and synovial membrane-derived MSCs *(5, 12, 14)*.

During embryonic development, WNT9A is sufficient to induce GDF5 expression in the joint interzones. Agrin and WNT9A alone or in combination induced GDF5 protein expression (Fig. 6H to I) and activated the CREB reporter assay (Fig 6J). Interestingly, agrin and WNT9A in combination induced activation of the CREB reporter assay more than agrin or WNT9A alone. The CREB inhibitor 666-15 negated the capacity of agrin to induce *GDF5* mRNA upregulation in C28/I2 cells (Fig. 6K), suggesting that the capacity of agrin to upregulate *GDF5* is CREB-dependent. Finally, overexpression of constitutively active LEF1, but not WNT3A, also negated agrin-induced *GDF5* upregulation (Fig. 6L to M). This does not necessarily mean that suppression of WNT signaling drives activation of *GDF5*, because caLEF1 overexpression also suppressed the capacity of agrin to induce CREB phosphorylation. Taken together, these results indicate that agrin

activates GDF5 expression and prompts chondrogenesis through activation of CREB-dependent transcription and suppression of canonical WNT signaling.

Agrin induces local accumulation of *Gdf5*-lineage joint stem cells and phosphorylation of CREB in vivo

To study whether the *Gdf5*-lineage of joint-specific MSCs contribute to agrin induced joint surface repair, we used transgenic mice harboring a tdTomato (Tom) cassette preceded by a LoxP-flanked stop cassette within the ROSA26 locus and Cre recombinase under the control of the *Gdf5* responsive elements active during embryonic development *(5, 50)*. In these *Gdf5*-Cre;Tom reporter mice, the progeny of cells that at any point during embryonic development have expressed *Gdf5* will express Tom, regardless of whether they still express *Gdf5*. Similar to our findings in wild type mice, agrin enhanced joint surface regeneration in *Gdf5*-Cre;Tom reporter mice (Fig 7A). Three weeks after surgery there was a marked increase in the number of Tom+ cells within the superficial portion of the repair tissue as well as in the synovial membrane of the mice that received agrin compared to controls (Fig. 7B to D). Co-immunofluorescence staining for Tom and collagen type II at eight weeks after injury revealed the presence of Tom+ chondrocytes embedded in a collagen type II-containing matrix along the joint surface of the repair tissue (Fig. 7E).

In keeping with our *in vitro* data, three weeks after surgery we detected a higher percentage of cells positive for pCREB within the repair tissue of agrin-treated animals (Fig. 7F and G). Dose response experiments using recombinant agrin revealed that concentrations between 1 and 1000 ng/ml suppressed WNT signaling and activated CREB signaling to a similar extent as COS7-

AGRIN cell lysates (fig. S6A and B). An injection of a collagen gel containing 100 ng/ml rAGRIN into osteochondral defects also led to increased Tom+ cells in the repair mesenchyme three weeks after surgery compared to PBS control (fig. S6, C to E), as observed with the COS7-AGRIN cell lysates.

Intra-articular agrin delivery improves long-term repair of critical size osteochondral defects and improves joint function in sheep.

Finally, we tested whether agrin could also support long-term cartilage repair in a large animal model. A critical-size osteochondral defect (8mm diameter and 5mm deep) was generated in the weight-bearing region of the medial femoral condyle of adult sheep. The defect was filled with a type I collagen gel containing either human full-length agrin or GFP as control. At 6 months post-surgery, μCT analysis revealed that bone repair was better in the agrin than the control group, as noted by reduced defect volume (Fig. 8A and B). The Pineda injury score revealed superior healing of the defect in the agrin group (Fig. 8C and D). Sheep that received the agrin-containing gel spent more time playing and less time resting throughout the study (Fig. 8E and F), suggesting that the improved repair was associated with improved function.

Discussion

We demonstrated that joint surface injury triggers expression of agrin, which in turn recruits chondrogenic GDF5 lineage joint-resident progenitor cells to the repair mesenchyme and enables the morphogenesis of joint surface. In critical size defects, which do not heal spontaneously, exogenous agrin induced GDF5 expression in joint-resident MSCs and triggered their chondrocytic differentiation by inhibiting WNT signaling downstream of β-catenin in a CREB-dependent manner (fig. S7). Tissue patterning requires temporal and spatial coordination of cell migration, proliferation and differentiation *(6, 10)*. The WNT, BMP and CREB-dependent signaling pathways are key players in the patterning and morphogenesis of synovial joints*(6, 51)* during embryonic development. Whereas the modulation of these pathways individually failed to result in morphogenesis -- for instance, BMP2 is chondrogenic but leads to ectopic cartilage and bone formation*(52)* -- exogenous agrin resulted in harmonious postnatal repair morphogenesis.

During embryonic development WNT9A is sufficient *(11)* but not required *(53)* to induce joint formation whereas GDF5 is required (at least for some joints) but not sufficient *(13, 54)*, because disruption of *Gdf5* in mice is not associated with joint fusion. It was previously thought that the *GDF5* lineage of progenitor cells was established early in development and that cells later migrated to the joint interzones, thereby contributing to the formation of the articular cartilage and ligaments *(12, 14)*. This concept was challenged by subsequent lineage-tracking experiments using an inducible system allowing genetic labeling of *Gdf5*-positive cells at different stages of development *(7)*. Such experiments demonstrated a continuous recruitment of *Gdf5*-lineage cells to the joint interzones throughout development. Cells entering the *Gdf5* lineage at different developmental stages contributed to different tissue structures within the joints. This new paradigm

is in keeping with our data showing recruitment of *Gdf5*-lineage cells to the site of injury induced by agrin even in adulthood. Agrin failed to induce GDF5 in bone marrow-derived MSCs, thereby suggesting that its function is specific to *GDF5*-lineage cells. This may explain why agrin, as opposed to other chondrogenic molecules such as BMPs and TGF-β *(55, 56)*, did not induce ectopic cartilage or bone formation.

Although both WNT9A and agrin induced GDF5 upregulation, the former is an activator of the canonical WNT signaling and inhibits chondrogenesis whereas the latter is an inhibitor of canonical WNT signaling and promotes chondrogenesis. WNT9A enhanced the capacity of agrin in activating CREB in HEK293 cells. The presence of a cAMP response element (CRE) in the *GDF5* promoter *(47)* suggests that CREB is a critical element for the capacity of agrin to upregulate GDF5.

Agrin inhibited canonical WNT signaling downstream of β-catenin. Such mechanism is independent of the ligands moiety and the WNT receptor repertoire and therefore overrides all other upstream regulation including activating mutations of β-catenin which result in cancer *(57)*. This property of agrin may open therapeutic opportunities for its use in other conditions such as osteoarthritis *(58)* and cancer *(57)*, in which downregulation of canonical WNT signaling is desirable without incurring compensatory mechanisms. Notably, WNT inhibition is currently being tested as a treatment for osteoarthritis *(59–62)*.

The capacity of agrin to induce long-term cartilage regeneration after a single administration makes it an excellent candidate for clinical use. One problem in clinical translation is manufacturing. In its fully glycosylated state, agrin is a large, poorly soluble molecule of ~500-600kD which is difficult to purify to clinical grade in a biologically active form. We have shown

that a purified C-terminal deletion mutant of only ~95kD is sufficient to induce chondrogenesis *in vitro* at least as potently as the full-length molecule, but the efficacy of such deletion needs to be confirmed *in vivo*, since the N-terminus contains domains responsible for binding to the extracellular matrix. Such domains, and the capacity of agrin to bind to the extracellular matrix, may be responsible for its remarkable long-term efficacy.

Another limitation of our study is that we applied agrin therapeutically shortly after surgical generation of osteochondral defects in otherwise normal knees. In human patients, cartilage defects are often associated with meniscal/ligament damage and sometimes with some degree of osteoarthritis. It is still to be proven whether agrin will be able to induce cartilage regeneration under these circumstances in which joint instability might be compromised, or in the presence of inflammation. Finally, accurate pharmacokinetic studies and dose responses will be needed to identify the optimal administration regimen.

No ectopic cartilage was observed after intraarticular delivery despite the chondrogenic capacity of agrin. This is in contrast with the abundant ectopic cartilage and bone formation observed after delivery of TGF-β or BMP2 *(56, 63)*. In addition, the chondrogenic and anabolic capacity of agrin could be detected consistently even in the presence of 10% fetal bovine serum, which overrides the anabolic capacity of TGF-β and BMPs *(64, 65)*. The capacity of agrin to preserve the architecture of the native tissue is distinct and of important translational relevance. We anticipate that the optimization of delivery will be key for the clinical translation in cartilage repair strategies.

Materials and Methods

Study design

The overall scope of this controlled laboratory study was to assess the effect of agrin in the regeneration of osteochondral defects and its mechanism of action. Human primary cells were obtained from patients undergoing joint replacement as described below according to ethics approval REC N. 07/Q0605/29. Cell lines were acquired commercially. Treatments, for each experiment, are detailed in the figure legends. Sample size of in vitro and in vivo experiments was determined by power calculations based on previous similar experiments to ensure a power of at least 0.8 in detecting an effect size of 0.5.

In vivo studies.

Preliminary efficacy study in Fig 5.

Wild type, 10 week old male C57BL/6 mice (4 animals per group, 4 joints analysed) were subjected to the generation of osteochondral defects as described below and the defect was filled immediately with either a collagen gel containing GFP (crude cell extract from transduced COS7 cells) or a collagen gel containing full length agrin (crude cell extract from transduced COS7 cells). The animals were killed 8 weeks after surgery.

Efficacy study in figure 7.

Female *Gdf5*-Cre;Tom reporter mice (age 10 week old, 8 mice per group) were subjected to the generation of bilateral osteochondral defects. The defects were filled immediately with either a collagen gel containing GFP (crude cell extract from transduced COS7 cells) or a collagen gel

containing full length agrin (crude cell extract from transduced COS7 cells). Three mice per group were killed 3 weeks after surgery and 5 mice per treatment group were killed after 8 weeks. One joint from the control group at 8 week time point was excluded from analysis because of an accidental cortical fracture during surgery.

Confirmation of recruitment of Gdf5-Tom+ cells using recombinant agrin (fig S6).

Eight *Gdf5*-Cre;Tom mice (2 females and 6 males; 3 males and 1female per treatment group) were subjected to the generation of bilateral osteochondral defects. The defects were filled immediately with either a collagen gel or a collagen gel containing 100 ng/ml of recombinant C-terminal agrin (rAGRIN). Animals were killed after 3 weeks and one joint per animal was processed for analysis.

Efficacy study in sheep (Fig. 8).

Twelve female sheep aged 2.9 years ± 0.41 (SD)were subjected to the generation of an osteochondral defect. The defects were filled immediately with either a collagen gel containing GFP (crude cell extract from transduced COS7 cells) or a collagen gel containing full length agrin (crude cell extract from transduced COS7 cells). In the GFP group 2 animals were excluded from the histological analysis, one because of osteomyelitis and one because of a subchondral cyst. All animals were killed 6 months after surgery.

In all animal studies, neither the operator nor the assessors were aware of the treatment. To minimize the risk that fights within individual cages skewed biased the results, treatment was randomized in each cage in the experiment with wild type mice. All sheep were kept in the same flock. The treatment table and the outcome tables were kept in separate databases until the outcomes had been recorded and only merged at the time of statistical analysis. Conditions to stop

collection of data and humane endpoints for mice included weight loss >15% or evidence of excoriating dermatitis for more than 1 week or of ulcerative dermatitis for any length but were never met. No mouse, therefore, was killed early or excluded from analysis. Three sheep developed large subchondral cysts as a complication of surgery, which were detected radiographically and were excluded from further analysis.

Cells, cell lines and expression vectors

Adult human articular cartilage and synovial membrane were obtained following informed consent from patients who underwent joint replacement for knee OA after obtaining informed consent (5 men and 3 women, with a mean ± SD age of 68 ± 7 years). All procedures were approved by the East London and The City Research Ethics Committee 3 (ethics approval REC N. 07/Q0605/29).

Articular chondrocytes and synovial membrane mesenchymal stem cells were isolated and expanded as previously described *(25, 31)*. Bovine chondrocytes were isolated from the metatarsal joints of 18-month-old bovine, obtained within 6hrs of death from a local abattoir, as previously described *(25)*, chondrocytes from three joints were pooled. C28/I2 chondrocytes *(66)* were a kind gift from Dr Mary Goldring (HSS Research Institute, Hospital for Special Surgery, New York, New York). COS-7 cells were a kind gift from Dr Michael Ferns (UC Davis Health system, USA). HEK293 cells were purchased from ATCC.

All cells were cultured in complete medium (DMEM/F-12, containing 10% FBS and 1% antibiotic antimycotic solution) (Thermo Fisher Scientific). COS-7 feeders producing agrin or GFP or TGF-

β were obtained as previously described *(25)*. Transfections were performed using JetPrime (Polyplus) according to the manufacturer's instructions.

With all cells, chondrogenesis was assessed in micromass culture as previously described *(25, 48, 67)*. Extracellular matrix deposition was quantified by staining with Alcian Blue 8 GS (Merck) at pH 0.2 followed by extraction in 8 M guanidine HCl (Thermo Fisher Scientific) and spectrophotometric quantitation at a wavelength of 630nm *(25, 48, 67)*. DNA was quantified using the Sybr Green method according to manufacturer's instruction (Origene).

The Rat Agrin plasmid *(68)* was a kind gift from Dr Michael Ferns (UC Davis Health system, USA). The Lrp4 plasmid *(23)* was a kind gift of Dr Lin Mei (Medical College of Georgia, Augusta, USA). TGF-β plasmid was a kind gift from Dr. Gerhard Gross. The caLEF1 and the caCTNNB1 plasmids were a kind gift from Dr. Carles Gasson-Massuet.

siRNA oligonucleotide sequences can be found in table S1. A Stealth RNAi negative control duplex of low guanine-cytosine (GC) content (Invitrogen) was used as a negative control for *AGRN* siRNA.

Generation of agrin-expressing COS7 cells and agrin-containing collagen gel

The full-length coding sequence of human agrin (accession N. AB191264) was cloned into the BamHI and Kpn1 site of the pLNTSFFV. The agrin sequence was synthesized in 3 parts by Gene-Art (Life Technologies). The 5' fragment was ligated into the BamHI/XhoI sites of the vector. The 3' fragment was the ligated into this plasmid at the XhoI and Kpn1 sites. Finally, the Xho1

fragment comprising the central portion of the gene was ligated into the XhoI site of the vector to give the complete cDNA. Lentiviruses were packaged in HEK 293T cells using standard procedures. The agrin lentivirus (or GFP lentivirus as control) was used to transduce COS7 cells, which were then cloned by limiting dilution. After three passages, the clone with the highest expression of agrin as determined by immunofluorescence was selected and used for further studies.

To generate collagen gel containing agrin (or GFP as control), agrin or GFP-overexpressing COS7 cells were washed twice in ice-cold PBS, detached mechanically with a cell scraper, resuspended in PBS, pelleted at 10000 g for 20 minutes and resuspended in an equal volume of PBS. The samples were subjected to 5 cycles of freeze-thawing alternating between liquid nitrogen and a 37°C water bath and finally diluted 1:1 in a 5 mg/ml solution of ice-cold type I rat tail collagen at pH 7.5 (Corning - 354249) prepared according to the manufacturer's instruction. The preparation was kept on ice to prevent polymerization until injected.

Generation of recombinant Agrin

Recombinant human non-neuronal C-terminal Agrin (rAGRIN) was generated as follows. The C-terminal portion of Agrin (AA 1244-2045 from GeneBank accession number BAD52440) was cloned by PCR from the backbone of the full-length human non-neuronal Agrin adenovirus and subcloned into a 3rd generation lentivirus gene expression vector backbone downstream of the CMV promoter, an IgG kappa signal peptide and followed by an enterokinase cleavage site, thermostable alkaline phosphatase, Myc and 10X His tags and finally by a stop codon. The

lentivirus backbone was transiently transfected into Expi293 cells (Thermo Fisher Scientific) using the Expi293 Expression System (Thermo Fisher Scientific) as per manufacturer's instructions. At day 3 post transfection, cell-free supernatant was collected and recombinant Agrin was recovered using His SpinTrap columns (GE Healthcare), according to manufacturer's instructions.

Animals and animal procedures

All animal procedures were subjected to local ethical approval and Home Office Licensing. Mouse experiments were regulated by PPL no. 70/7986 and 60/4528, sheep experiments by PPL no. 70/7740. C57BL/6 mice were purchased from Charles River UK. *Gdf5*-Cre;Tom mice *(5)* were generated by crossing *Gdf5*-Cre transgenics (Tg(*Gdf5*-Cre-ALPP)1Kng) *(14)* (Kind gift of Dr D. Kingsley, Stanford, CA, USA) with Cre-inducible tdTomato (Tom) reporter mice (B6.Cg-Gt(ROSA) 26Sortm14(CAG-tdTomato)Hze/J) (Jackson Laboratories). *Gdf5*-Cre;Tom mice were on a mixed FVB/C57BL/6 background. All mice were maintained in isolator cages or standard housing in groups of 3-5 and fed ad libitum.

Murine model of osteochondral defect repair

Mice were anesthetized with isofluorane. The knees were shaved and disinfected with 70% ethanol. The skin was cut with fine scissors and separated from the underlying tissue by blunt dissection. The femur was placed so that the shaft was perfectly vertical, with the knee flexed at 90°. A 25G needle (Terumo Agani G25, cannula 0.5mm, length 25mm, bevel 11°) was placed on

the lateral condyle in correspondence of the intersection of a vertical line tangent to the lateral margin of the patella and a horizontal line tangent to the inferior margin of the patella. By applying gentle pressure and rotation, the needle was driven through the joint capsule, the cartilage, and the bone, while aiming for the center of the femoral shaft. As soon as the bevel of the needle was completely buried, the G25 needle was retracted and replaced with a G21 needle (Terumo Agani, G21, cannula 0.8 mm, length 50 mm, bevel 11°). The G21 needle was again gently rotated and advanced until its bevel was completely hidden. The G21 was retracted while still turning to extract the bone debris and leaving a cavity. If there was any bleeding, this was blotted with sterile gauze. Liquid collagen type I gel containing the lysate of COS7 cells overexpressing full-length human agrin(crude extract from transduced COS7 cells)accession No. AB191264) or recombinant C-terminal agrin as indicated, or GFP (crude extract from transduced COS7 cells) or PBS as indicated, was injected using a pulled glass pipette tip with a diameter of approximately 10µm mounted at the end of a regular 2 µl pipette tip until the defect was full. After waiting approximately 20 seconds to allow the gel to set, the joint capsule was closed with a single suture with Vycril 6-0 and the skin was closed with an interrupted suture (Ethilon 5-0 a-traumatic needle). After recovery mice, fed *ad libitum* in individually filtered cages (3-5 mice per cage). For wildtype mice, treatments were randomized within each cage. The animals were monitored post-operatively for signs of suffering and local infection. The operator and the scorers were blind to the treatment.

At the stated time points mice were killed, the joint dissected and processed for histology. Sagittal sections through the center of the defect were identified as the first section that, starting from the lateral side, intersected the lateral margin of the patellar bone. Such sections were stained with Safranin O and scored using the Pineda score *(49)*.

Ovine model of osteochondral defect repair

Adult [aged 2.9 years ± 0.41 (SD); individual ages can be found in table S1] female sheep were anesthetized with isoflurane. Following a sterile preparation of the skin, the joint was opened using a lateral para-patella approach. An 8 mm diameter, 5 mm deep osteochondral defect was created using a hand drill. The defect was lavaged to remove debris. Defects were filled with liquid collagen type I gel containing the lysate of COS7 cells overexpressing full length human agrin or GFP as control. After waiting about 20 seconds to allow the gel to set, the capsule was closed using 3M Monocryl in an interrupted mattress pattern. The skin was closed with 2M Vicryl. Sheep were recovered and then housed for two weeks post-surgery indoors in pens. Carprofen was administered at a dose of 4 mg/kg at the time of surgery then 4 mg/kg once a day for three days post-surgery. After this time, sheep were kept in one flock in a field to allow free and natural movement. At 6 months post-surgery sheep were killed, the knees processed for μCT and subsequently processed for histology. Mid-defect sections were stained and scored as described above.

For μCT analysis, sheep knee joints were scanned using a Nikon XT H 225 ST CT scanner. Reconstruction was done using CT Pro V2.2 Nikon software (Nikon Metrology UK Ltd) and the images were saved as a tif series. These were then viewed using Dataviewer v1.5 software (Bruker, Kontich). To allow subsequent analysis the data was then resaved as a transaxial (x,y) dataset. This new dataset was then opened in CTAn (v1.13) (Bruker, Kontich). Before analysis was carried out the true pixel value from the Nikon scan was manually added using the image properties option, as the calibration was not automatically saved. A region of interest was drawn to define the defect

area in each joint, from which the defect volume was determined. The person analyzing the µCT data was blinded to the study groups.

Histology and immunostainings

All samples were fixed in 4% paraformaldehyde at 4°C overnight, decalcified in 10% EDTA in PBS for 2 weeks at 4°C (*Gdf5*-Cre;Tom) or in 33% Formic Acid for 24hrs and then washed for 24hrs in water at room temperate (wildtype), dehydrated in an ethanol series, embedded in paraffin and 5 µm sections were obtained. Safranin O staining (pH 4.2) or toluidine blue (pH 4.5) was performed according to standard protocols.

Immunofluorescence and immunohistochemical, staining was carried out as previously described *(25, 48)*. For antigen retrieval on paraffin sections pepsin digestion was performed. Where phosphatase treatment was carried out, sections were incubated with Lambda phosphatase for 2hrs at 37°C according to manufacturer's instructions (CST). Antibodies and dilutions used are provided in table S2. Tissue staining was carried out using an overnight incubation of the primary antibody at 4°C, immunocytochemistry was performed following 1hr incubation at room temperature. Sections were counterstained with hematoxylin or with 4′,6-diamidino-2-phenylindole (DAPI) (Life Technologies). Slides were mounted in Mowiol (EMD Millipore, Darmstadt), and images were acquired with a fluorescence microscope (BX61; Olympus) using a Uplan-Fluor 40× NA 0.85 objective lens, a Zeiss 710 META Laser-Scanning Confocal Microscope (Carl Zeiss Ltd), or a Zeiss Axioscan Z1 slide scanner (Carl Zeiss Ltd). Images were acquired by using an F-View II Soft Imaging Solutions (SIS) camera and Cell P software

(Olympus), or using ZEN software (Carl Zeiss Ltd). Image contrast was modified with Photoshop 7.0 for best graphic rendering, equally for all treatments.

Histomorphometry

Histomorphometry was performed with ImageJ software (NIH). The number of cells positive for phospho-CREB (pCREB) was calculated as follows. Images of immunohistochemistry counterstained with hematoxylin were opened in ImageJ *(69)*. All cells (positive and negative) were selected using the color threshold tool (Image>Adjust>Color threshold). The tool was set on the RGB color space and all three (red, blue and green) channels were passed, ensuring that the blue channel (hematoxylin positive cells) was passed with the upper limit on the peak of the histogram. The passed component of the image was sampled and pasted on a new image. Such image contained all cells, positive (brown) and negative (blue) and no background. This image was converted to 8 bit and thresholded in such a way to maximize separation of adjacent cells while still selecting every cell. A further deconvolution of overlapping cells was obtained using the watershed tool (Process>binary>watershed). Total cells were then counted with the Analyze Particles tool (Analyze>Analyze Particles). Care was taken to optimize the size of the particles to count so to exclude specks that did not reach the minimum size of a cell. In our case we used 100 px~infinity. The positive cells were counted in the same way except that during colour thresholding, the upper limit of the blue channel was placed immediately to the left of the blue histogram, so that all blue cells were thresholded out and the resulting image only contained brown cells. The counts were expressed as (positive/total cells) x100.

The number of cells positive for Tomato in immunohistochemistry could not be quantified in the same way because the cytoplasmic staining of neighboring cells could not always reliably be deconvoluted. Therefore, the area occupied by brown (immunohistochemistry) or blue (hematoxylin) staining was considered as proportional to the positive and negative cells. Image processing for this analysis was similar to that described above for phospho-CREB staining, with the following differences. First, after color thresholding, the second round of thresholding was performed so to include the entire histogram of the 8-bit images so not to alter the area occupied by any positive staining in the 8-bit images. Second, instead of the particle count, we used the "total area" of the results from "Analyze Particles" as (total area total cells/total area positive cells) x100.

Western blotting

Cells were washed in ice-cold PBS and lysed in ice-cold RIPA Buffer in the presence of protease and phosphatase inhibitors (Sigma) for 20 mins on ice. Protein concentrations were determined by bicinchoninic acid protein assay (Pierce). Samples were prepared for SDS-PAGE on 10% (wt/vol) Bis-Tris NuPAGE gels (Invitrogen) and transferred to nitrocellulose membrane. Blots were blocked in 5% BSA in 0.1% TBS-Tween) and incubated with primary antibodies at the concentrations stated in supplementary table I overnight at 4°C. After three washes in 0.1% TBST, blots were incubated for one hour at room temperature with HRP-conjugated secondary IgG (Dako). After further three washes, protein bands were visualized by chemiluminescence (Luminata Forte; Merk Millipore) using FluorChem E imaging system (Protein Simple). Measurements of band densitometry and quantification of protein expression was conducted using

ImageJ (NIH) *(69)*. Phospho protein expression was normalized to total protein levels and to α-TUBULIN (endogenous loading control).

Reporter assays

Subconfluent cells were co-transfected with SUPER8XTOPFlash *(34)* TCF/LEF–firefly luciferase reporter vector (Addgene) and CMV-Renilla luciferase vector (in a ratio 1:100). 24hrs after transfection, the medium was replaced and the cells were treated for 24hrs as specified. Luciferase activity was measured using the Dual Luciferase Reporter Assay System (Promega) in a TD-20/20 Luminometer (Turner Designs). Firefly luciferase activity was normalized by Renilla luciferase activity and expressed as relative luciferase units. See table S3 for all reagents.

Gene expression analysis

RNA extraction was performed using Trizol (Invitrogen) according to the manufacturer's instruction. Reverse transcription and real-time PCR were performed as previously described *(25)*. Primers and amplicon length are listed in table S4.

Microarray data from previously published datasets *(30)* were accessed through the Gene Expression Omnibus database at NIH (GEO accession GSE75181). Briefly, normalized data were downloaded from GEO as an expression dataset; the samples of interest (IL-1β-treated and control) were selected and gene expression was compared by fitting a linear model independently for each probe, with group as the *y* variable, using 'lmfit' ('limma' R package). The linear fit for each comparison was subsequently modified using the empirical Bayes ('eBayes') approach. For each

comparison, log_2 fold-change (logFC), P value, and adjusted P value (false discovery rate, FDR for multiple comparisons) was output. Individual samples expression data for agrin were extracted from the expression dataset and the statistics obtained from the statistics output and used to build the graph. To facilitate the reproduction of the data, an R script is supplied in supplementary materials to obtain the raw data, select the samples of interest, perform the statistical analysis and generate the graph. Pre-processed, normalized data for individual genes were obtained using the GEO2R functionality.

Statistical analysis

Means of parametric data were compared with a student's t test or with ANOVA followed by Tukey HSD post hoc test for multiple comparisons. When necessary, log or square root transformation was applied to correct skewed distributions in order to satisfy the assumptions of parametric tests. Non-parametric data were analyzed with the Mann-Whitney U test or, for multiple comparisons, the Kruskal Wallis test followed by the Dunn test. Dose response curves and repeated measures were assessed by two-way ANOVA and, if different treatments were applied, ANCOVA followed by Tukey HSD for multiple comparisons. Statistical analysis was performed using either R or GraphPad Prism software. Data shown as box and whisker blot. Box extends from the 25th to 75th percentiles. Error lines represent max to min points. *P* values <0.05 were considered significant.

References

1. N. Verzijl, J. DeGroot, S. R. Thorpe, R. A. Bank, J. N. Shaw, T. J. Lyons, J. W. J. Bijlsma, F. P. J. G. Lafeber, J. W. Baynes, J. M. TeKoppele, Effect of Collagen Turnover on the Accumulation of Advanced Glycation End Products, *J. Biol. Chem.* **275**, 39027–39031 (2000).

2. M. Hiligsmann, C. Cooper, N. Arden, M. Boers, J. C. Branco, M. Luisa Brandi, O. Bruyère, F. Guillemin, M. C. Hochberg, D. J. Hunter, J. A. Kanis, T. K. Kvien, A. Laslop, J.-P. Pelletier, D. Pinto, S. Reiter-Niesert, R. Rizzoli, L. C. Rovati, J. L. H. (Hans) Severens, S. Silverman, Y. Tsouderos, P. Tugwell, J.-Y. Reginster, Health economics in the field of osteoarthritis: an expert's consensus paper from the European Society for Clinical and Economic Aspects of Osteoporosis and Osteoarthritis (ESCEO)., *Semin. Arthritis Rheum.* **43**, 303–13 (2013).

3. W. W. Curl, J. Krome, E. S. Gordon, J. Rushing, B. P. Smith, G. G. Poehling, Cartilage injuries: A review of 31,516 knee arthroscopies, *Arthrosc. J. Arthrosc. Relat. Surg.* **13**, 456–460 (1997).

4. K. Hjelle, E. Solheim, T. Strand, R. Muri, M. Brittberg, Articular cartilage defects in 1,000 knee arthroscopies., *Arthroscopy* **18**, 730–4 (2002).

5. A. J. Roelofs, J. Zupan, A. H. K. Riemen, K. Kania, S. Ansboro, N. White, S. M. Clark, C. De Bari, C. De Bari, Joint morphogenetic cells in the adult mammalian synovium, *Nat. Commun.* **8** (2017), doi:10.1038/ncomms15040.

6. R. S. Decker, Articular cartilage and joint development from embryogenesis to adulthood, *Semin. Cell Dev. Biol.* **62**, 50–56 (2017).

7. Y. Shwartz, S. Viukov, S. Krief, E. Zelzer, Joint Development Involves a Continuous Influx of Gdf5-Positive Cells, *Cell Rep.* **15**, 2577–2587 (2016).

8. F. Dell'Accio, T. L. Vincent, Joint surface defects: clinical course and cellular response in spontaneous and experimental lesions., *Eur. Cell. Mater.* **20**, 210–7 (2010).

9. N. M. Eltawil, C. De Bari, P. Achan, C. Pitzalis, F. Dell'accio, A novel in vivo murine model of cartilage regeneration. Age and strain-dependent outcome after joint surface injury., *Osteoarthritis Cartilage* **17**, 695–704 (2009).

10. Y. Anraku, H. Mizuta, A. Sei, S. Kudo, E. Nakamura, K. Senba, Y. Hiraki, Analyses of early events during chondrogenic repair in rat full-thickness articular cartilage defects, **27**, 272–286 (2009).

11. C. Hartmann, C. J. Tabin, Wnt-14 plays a pivotal role in inducing synovial joint formation in the developing appendicular skeleton., *Cell* **104**, 341–51 (2001).

12. E. Koyama, Y. Shibukawa, M. Nagayama, H. Sugito, B. Young, T. Yuasa, T. Okabe, T. Ochiai, N. Kamiya, R. B. Rountree, D. M. Kingsley, M. Iwamoto, M. Enomoto-Iwamoto, M. Pacifici, A distinct cohort of progenitor cells participates in synovial joint and articular cartilage formation during mouse limb skeletogenesis., *Dev. Biol.* **316**, 62–73 (2008).

13. E. E. Storm, T. V Huynh, N. G. Copeland, N. A. Jenkins, D. M. Kingsley, S. J. Lee, Limb alterations in brachypodism mice due to mutations in a new member of the TGF beta-superfamily., *Nature* **368**, 639–43 (1994).

14. R. B. Rountree, M. Schoor, H. Chen, M. E. Marks, V. Harley, Y. Mishina, D. M. Kingsley, BMP receptor signaling is required for postnatal maintenance of articular cartilage., *PLoS Biol.* **2**, e355 (2004).

15. X. Guo, T. F. Day, X. Jiang, L. Garrett-Beal, L. Topol, Y. Yang, Wnt/beta-catenin signaling is sufficient and necessary for synovial joint formation., *Genes Dev.* **18**, 2404–17 (2004).

16. R. Yasuhara, Y. Ohta, T. Yuasa, N. Kondo, T. Hoang, S. Addya, P. Fortina, M. Pacifici, M. Iwamoto, M. Enomoto-Iwamoto, Roles of β-catenin signaling in phenotypic expression and proliferation of articular cartilage superficial zone cells., *Lab. Invest.* **91**, 1739–52 (2011).

17. J. Loughlin, B. Dowling, K. Chapman, L. Marcelline, Z. Mustafa, L. Southam, A. Ferreira, C. Ciesielski, D. A. Carson, M. Corr, Functional variants within the secreted frizzled-related protein 3 gene are associated with hip osteoarthritis in females., *Proc. Natl. Acad. Sci. U. S. A.* **101**, 9757–62 (2004).

18. R. J. U. Lories, J. Peeters, A. Bakker, P. Tylzanowski, I. Derese, J. Schrooten, J. T. Thomas, F. P. Luyten, Articular cartilage and biomechanical properties of the long bones in Frzb-knockout mice., *Arthritis Rheum.* **56**, 4095–103 (2007).

19. K. Willert, R. Nusse, Wnt proteins., *Cold Spring Harb. Perspect. Biol.* **4**, a007864 (2012).

20. R. van Amerongen, Alternative Wnt pathways and receptors., *Cold Spring Harb. Perspect. Biol.* **4** (2012), doi:10.1101/cshperspect.a007914.

21. G. Nalesso, J. Sherwood, J. Bertrand, T. Pap, M. Ramachandran, C. De Bari, C. Pitzalis, F. Dell'accio, B. C. De, WNT-3A modulates articular chondrocyte phenotype by activating both canonical and noncanonical pathways., *J. Cell Biol.* **193**, 551–64 (2011).

22. J. T. Campanelli, W. Hoch, F. Rupp, T. Kreiner, R. H. Scheller, Agrin mediates cell contact-induced acetylcholine receptor clustering., *Cell* **67**, 909–16 (1991).

23. B. Zhang, S. Luo, Q. Wang, T. Suzuki, W. C. Xiong, L. Mei, LRP4 serves as a coreceptor of agrin., *Neuron* **60**, 285–97 (2008).

24. J. T. Campanelli, M. Ferns, W. Hoch, F. Rupp, M. von Zastrow, Z. Hall, R. H. Scheller, Agrin: a synaptic basal lamina protein that regulates development of the neuromuscular

669 junction., *Cold Spring Harb. Symp. Quant. Biol.* **57**, 461–72 (1992).

670 25. S. Eldridge, G. Nalesso, H. Ismail, K. Vicente-Greco, P. Kabouridis, M. Ramachandran, A.
671 Niemeier, J. Herz, C. Pitzalis, M. Perretti, F. Dell'Accio, Agrin mediates chondrocyte
672 homeostasis and requires both LRP4 and α-dystroglycan to enhance cartilage formation in vitro
673 and in vivo, *Ann. Rheum. Dis.* **75**, 1228–1235 (2016).

674 26. F. Dell'Accio, C. De Bari, N. M. Eltawil, P. Vanhummelen, C. Pitzalis, B. C. De,
675 Dell'Accio, C. De Bari, N. M. Eltawil, P. Vanhummelen, C. Pitzalis, B. C. De, Identification of
676 the molecular response of articular cartilage to injury, by microarray screening: Wnt-16
677 expression and signaling after injury and in osteoarthritis., *Arthritis Rheum.* **58**, 1410–21 (2008).

678 27. S. Eldridge, G. Nalesso, H. Ismail, K. Vicente-Greco, P. Kabouridis, M. Ramachandran, A.
679 Niemeier, J. Herz, C. Pitzalis, M. Perretti, F. Dell'Accio, F. Dell'Accio, Agrin mediates
680 chondrocyte homeostasis and requires both LRP4 and α-dystroglycan to enhance cartilage
681 formation in vitro and in vivo, *Ann.Rheum.Dis.* **75**, 1228–35 (2016).

682 28. J. B. Fitzgerald, M. Jin, D. Dean, D. J. Wood, M. H. Zheng, A. J. Grodzinsky, Mechanical
683 Compression of Cartilage Explants Induces Multiple Time-dependent Gene Expression Patterns
684 and Involves Intracellular Calcium and Cyclic AMP, *J. Biol. Chem.* **279**, 19502–19511 (2004).

685 29. J. Gruber, T. L. Vincent, M. Hermansson, M. Bolton, R. Wait, J. Saklatvala, Induction of
686 interleukin-1 in articular cartilage by explantation and cutting, **50**, 2539–2546 (2004).

687 30. F. Comblain, J.-E. Dubuc, C. Lambert, C. Sanchez, I. Lesponne, S. Serisier, Y. Henrotin, M.
688 Lammi, Ed. Identification of Targets of a New Nutritional Mixture for Osteoarthritis
689 Management Composed by Curcuminoids Extract, Hydrolyzed Collagen and Green Tea Extract,
690 *PLoS One* **11**, e0156902 (2016).

691 31. C. De Bari, F. Dell'Accio, P. Tylzanowski, F. P. Luyten, Multipotent mesenchymal stem
692 cells from adult human synovial membrane., *Arthritis Rheum.* **44**, 1928–42 (2001).

693 32. N. Asai, B. Ohkawara, M. Ito, A. Masuda, N. Ishiguro, K. Ohno, LRP4 induces extracellular
694 matrix productions and facilitates chondrocyte differentiation., *Biochem. Biophys. Res. Commun.*
695 **451**, 302–7 (2014).

696 33. H. Y. Choi, M. Dieckmann, J. Herz, A. Niemeier, E. A. A. Nollen, Ed. Lrp4, a Novel
697 Receptor for Dickkopf 1 and Sclerostin, Is Expressed by Osteoblasts and Regulates Bone Growth
698 and Turnover In Vivo, *PLoS One* **4**, e7930 (2009).

699 34. M. T. Veeman, D. C. Slusarski, A. Kaykas, S. H. Louie, R. T. Moon, Zebrafish Prickle, a
700 Modulator of Noncanonical Wnt/Fz Signaling, Regulates Gastrulation Movements, *Curr. Biol.*
701 **13**, 680–685 (2003).

702 35. M. Aoki, A. Hecht, U. Kruse, R. Kemler, P. K. Vogt, Nuclear endpoint of Wnt signaling:
703 neoplastic transformation induced by transactivating lymphoid-enhancing factor 1, *Proc. Natl.*
704 *Acad. Sci. U. S. A.* **96**, 139–144 (1999).

705 36. N. Sato, L. Meijer, L. Skaltsounis, P. Greengard, A. H. Brivanlou, Maintenance of
706 pluripotency in human and mouse embryonic stem cells through activation of Wnt signaling by a
707 pharmacological GSK-3-specific inhibitor, *Nat. Med.* **10**, 55–63 (2004).

708 37. J. Gwak, S. G. Hwang, H.-S. S. Park, S. R. Choi, S.-H. H. Park, H. Kim, N.-C. C. Ha, S. J.
709 Bae, J.-K. K. Han, D.-E. E. Kim, J. W. Cho, S. Oh, Small molecule-based disruption of the
710 Axin/beta-catenin protein complex regulates mesenchymal stem cell differentiation, *Cell Res* **22**,
711 237–247 (2012).

712 38. A. I. M. Barth, D. B. Stewart, W. J. Nelson, T cell factor-activated transcription is not

713 sufficient to induce anchorage-independent growth of epithelial cells expressing mutant -catenin,
714 *Proc. Natl. Acad. Sci.* **96**, 4947–4952 (1999).

715 39. C. Chiamulera, M. Di Chio, V. Tedesco, C. Cantù, E. Formaggio, G. Fumagalli, Nicotine-
716 induced phosphorylation of phosphorylated cyclic AMP response element-binding protein
717 (pCREB) in hippocampal neurons is potentiated by agrin, *Neurosci. Lett.* **442**, 234–238 (2008).

718 40. L. G. W. Hilgenberg, M. A. Smith, Agrin signaling in cortical neurons is mediated by a
719 tyrosine kinase-dependent increase in intracellular Ca2+ that engages both CaMKII and MAPK
720 signal pathways, *J. Neurobiol.* **61**, 289–300 (2004).

721 41. Q.-B. B. Tian, T. Suzuki, T. Yamauchi, H. Sakagami, Y. Yoshimura, S. Miyazawa, K.
722 Nakayama, F. Saitoh, J.-P. P. Zhang, Y. Lu, H. Kondo, S. Endo, Interaction of LDL receptor-
723 related protein 4 (LRP4) with postsynaptic scaffold proteins via its C-terminal PDZ domain-
724 binding motif, and its regulation by Ca2+/calmodulin-dependent protein kinase II, *Eur. J.*
725 *Neurosci.* **23**, 2864–2876 (2006).

726 42. M. R. Montminy, L. M. Bilezikjian, Binding of a nuclear protein to the cyclic-AMP response
727 element of the somatostatin gene, *Nature* **328**, 175–178 (1987).

728 43. F. Xie, B. X. Li, A. Kassenbrock, C. Xue, X. Wang, D. Z. Qian, R. C. Sears, X. Xiao,
729 Identification of a Potent Inhibitor of CREB-Mediated Gene Transcription with Efficacious in
730 Vivo Anticancer Activity, *J. Med. Chem.* **58**, 5075–5087 (2015).

731 44. J. Y. Altarejos, M. Montminy, CREB and the CRTC co-activators: sensors for hormonal and
732 metabolic signals, *Nat. Rev. Mol. Cell Biol.* **12**, 141–151 (2011).

733 45. V. K. Raker, C. Becker, K. Steinbrink, The cAMP Pathway as Therapeutic Target in
734 Autoimmune and Inflammatory Diseases, *Front. Immunol.* **7** (2016),

735 doi:10.3389/fimmu.2016.00123.

736 46. K. YAN, L.-N. GAO, Y.-L. CUI, Y. ZHANG, X. ZHOU, The cyclic AMP signaling
737 pathway: Exploring targets for successful drug discovery (Review), *Mol. Med. Rep.* **13**, 3715–
738 3723 (2016).

739 47. X. Zhang, D. T. Odom, S.-H. Koo, M. D. Conkright, G. Canettieri, J. Best, H. Chen, R.
740 Jenner, E. Herbolsheimer, E. Jacobsen, S. Kadam, J. R. Ecker, B. Emerson, J. B. Hogenesch, T.
741 Unterman, R. A. Young, M. Montminy, Genome-wide analysis of cAMP-response element
742 binding protein occupancy, phosphorylation, and target gene activation in human tissues, *Proc.*
743 *Natl. Acad. Sci.* **102**, 4459–4464 (2005).

744 48. G. Nalesso, B. L. Thomas, J. C. Sherwood, J. Yu, O. Addimanda, S. E. Eldridge, A.-S.
745 Thorup, L. Dale, G. Schett, J. Zwerina, N. Eltawil, C. Pitzalis, F. Dell'Accio, WNT16
746 antagonises excessive canonical WNT activation and protects cartilage in osteoarthritis, *Ann.*
747 *Rheum. Dis.* , annrheumdis-2015-208577 (2017).

748 49. S. Pineda, A. Pollack, S. Stevenson, V. Goldberg, A. Caplan, A semiquantitative scale for
749 histologic grading of articular cartilage repair, *Acta Anat. (Basel).* **143**, 335–340 (1992).

750 50. S. K. Pregizer, A. M. Kiapour, M. Young, H. Chen, M. Schoor, Z. Liu, J. Cao, V. Rosen, T.
751 D. Capellini, Impact of broad regulatory regions on Gdf5 expression and function in knee
752 development and susceptibility to osteoarthritis, *Ann. Rheum. Dis.* **77**, 450–450 (2018).

753 51. F. Long, E. Schipani, H. Asahara, H. Kronenberg, M. Montminy, The CREB family of
754 activators is required for endochondral bone development, *Development* **128**, 541–550 (2001).

755 52. E. N. B. Davidson, E. L. Vitters, M. B. Bennink, P. L. E. M. van Lent, A. P. M. van Caam,
756 A. B. Blom, W. B. van den Berg, F. A. J. van de Loo, P. M. van der Kraan, E. N. Blaney

Davidson, E. L. Vitters, M. B. Bennink, P. L. E. M. van Lent, A. P. M. van Caam, A. B. Blom, W. B. van den Berg, F. A. J. van de Loo, P. M. van der Kraan, E. N. B. Davidson, P. L. E. M. Van Lent, A. P. M. Van Caam, W. B. Van Den Berg, F. A. J. Van De Loo, P. M. Van Der Kraan, Inducible chondrocyte-specific overexpression of BMP2 in young mice results in severe aggravation of osteophyte formation in experimental OA without altering cartilage damage., *Ann. Rheum. Dis.* **74**, 1257–64 (2014).

53. D. Später, T. P. Hill, R. J. O'sullivan, M. Gruber, D. A. Conner, C. Hartmann, Wnt9a signaling is required for joint integrity and regulation of Ihh during chondrogenesis, *Development* **133**, 3039–3049 (2006).

54. J. T. Thomas, M. W. Kilpatrick, K. Lin, L. Erlacher, P. Lembessis, T. Costa, P. Tsipouras, F. P. Luyten, Disruption of human limb morphogenesis by a dominant negative mutation in CDMP1, *Nat. Genet.* **17**, 58–64 (1997).

55. E. N. Blaney Davidson, E. L. Vitters, M. B. Bennink, P. L. E. M. van Lent, A. P. M. van Caam, A. B. Blom, W. B. van den Berg, F. A. J. van de Loo, P. M. van der Kraan, Inducible chondrocyte-specific overexpression of BMP2 in young mice results in severe aggravation of osteophyte formation in experimental OA without altering cartilage damage, *Ann. Rheum. Dis.* **74**, 1257–1264 (2015).

56. E. N. Blaney Davidson, E. L. Vitters, P. M. van der Kraan, W. B. van den Berg, Expression of transforming growth factor-beta (TGFbeta) and the TGFbeta signalling molecule SMAD-2P in spontaneous and instability-induced osteoarthritis: role in cartilage degradation, chondrogenesis and osteophyte formation., *Ann. Rheum. Dis.* **65**, 1414–21 (2006).

57. J. Rapp, L. Jaromi, K. Kvell, G. Miskei, J. E. Pongracz, WNT signaling - lung cancer is no exception., *Respir. Res.* **18**, 167 (2017).

780 58. M. Corr, Wnt-beta-catenin signaling in the pathogenesis of osteoarthritis., *Nat. Clin. Pract.*
781 *Rheumatol.* **4**, 550–6 (2008).

782 59. V. Deshmukh, H. Hu, C. Barroga, C. Bossard, S. KC, L. Dellamary, J. Stewart, K. Chiu, M.
783 Ibanez, M. Pedraza, T. Seo, L. Do, S. Cho, J. Cahiwat, B. Tam, J. R. S. Tambiah, J. Hood, N. E.
784 Lane, Y. Yazici, A small-molecule inhibitor of the Wnt pathway (SM04690) as a potential
785 disease modifying agent for the treatment of osteoarthritis of the knee, *Osteoarthr. Cartil.* **26**,
786 18–27 (2018).

787 60. V. Deshmukh, A. L. O'Green, C. Bossard, T. Seo, L. Lamangan, M. Ibanez, A. Ghias, C.
788 Lai, L. Do, S. Cho, J. Cahiwat, K. Chiu, M. Pedraza, S. Anderson, R. Harris, L. Dellamary, S.
789 KC, C. Barroga, B. Melchior, B. Tam, S. Kennedy, J. Tambiah, J. Hood, Y. Yazici, Modulation
790 of the Wnt pathway through inhibition of CLK2 and DYRK1A by lorecivivint as a novel,
791 potentially disease-modifying approach for knee osteoarthritis treatment, *Osteoarthr. Cartil.* **27**,
792 1347–1360 (2019).

793 61. Y. Yazici, T. E. McAlindon, R. Fleischmann, A. Gibofsky, N. E. Lane, A. J. Kivitz, N.
794 Skrepnik, E. Armas, C. J. Swearingen, A. DiFrancesco, J. R. S. Tambiah, J. Hood, M. C.
795 Hochberg, A novel Wnt pathway inhibitor, SM04690, for the treatment of moderate to severe
796 osteoarthritis of the knee: results of a 24-week, randomized, controlled, phase 1 study.,
797 *Osteoarthr. Cartil.* **11**, 716–724 (2017).

798 62. S. Monteagudo, F. M. F. Cornelis, C. Aznar-Lopez, P. Yibmantasiri, L.-A. Guns, P.
799 Carmeliet, F. Cailotto, R. J. Lories, DOT1L safeguards cartilage homeostasis and protects
800 against osteoarthritis, *Nat. Commun.* **8**, 15889 (2017).

801 63. P. M. van der Kraan, E. N. Blaney Davidson, W. B. van den Berg, Bone morphogenetic
802 proteins and articular cartilage: To serve and protect or a wolf in sheep clothing's?,

Osteoarthritis Cartilage **18**, 735–41 (2010).

64. F. P. Luyten, Y. M. Yu, M. Yanagishita, S. Vukicevic, R. G. Hammonds, A. H. Reddi, Natural bovine osteogenin and recombinant human bone morphogenetic protein-2B are equipotent in the maintenance of proteoglycans in bovine articular cartilage explant cultures., *J. Biol. Chem.* **267**, 3691–5 (1992).

65. S. Vukicevic, K. T. Sampath, Eds., *Bone Morphogenetic Proteins: Regeneration of Bone and Beyond* (Birkhäuser Basel, Basel, 2004; http://link.springer.com/10.1007/978-3-0348-7857-9).

66. M. B. Goldring, J. R. Birkhead, L. F. Suen, R. Yamin, S. Mizuno, J. Glowacki, J. L. Arbiser, J. F. Apperley, Interleukin-1 beta-modulated gene expression in immortalized human chondrocytes, *J. Clin. Invest.* **94**, 2307–2316 (1994).

67. C. De Bari, F. Dell'Accio, F. P. Luyten, Human periosteum-derived cells maintain phenotypic stability and chondrogenic potential throughout expansion regardless of donor age., *Arthritis Rheum.* **44**, 85–95 (2001).

68. M. J. Ferns, J. T. Campanelli, W. Hoch, R. H. Scheller, Z. Hall, The ability of agrin to cluster AChRs depends on alternative splicing and on cell surface proteoglycans., *Neuron* **11**, 491–502 (1993).

69. C. A. Schneider, W. S. Rasband, K. W. Eliceiri, NIH Image to ImageJ: 25 years of image analysis, *Nat. Methods* **9**, 671–675 (2012).

Acknowledgments: We thank Prof. F. Luyten and Prof. C. Hartman for the critical reading of

this manuscript. The authors thank Technical Staff in the ARM Lab and Staff at the University of Aberdeen's Animal Facility and Microscopy & Histology Facility for their support.

Funding: We gratefully acknowledge funding support of this work by the MRC (MR/L022893/1, MR/N010973/1, MR/P026362/1), Versus Arthritis (19667, 21515, 20886, 21621), Rosetrees Trust (A1205), the Medical College of St Bartholomew's Hospital Trust and the William Harvey Research Foundation.

Author contributions: S.E.E. and F.D. designed the study. S.E.E., F.D., A.J.R., C.D.B., A.W.M., F.H., B.L.T., A-S.T., C.P. and J.W. contributed to the experimental design. S.E.E., F.D., A.B., H.W., M.K., G.Z., H.L., S.C., D.S., A.A., K.S., J.W., B.F.F. and F.H. performed experiments. Data was interpreted by S.E.E., F.D.., A-S.T., A.J.R., C.D.B., F.H. and B.L.T. S.E.E., F.D., A.J.R. and C.D.B. contributed to writing the manuscript.

Competing interests: FD has received consultancy fees from Samumed and UCB. FD and SE have filed a patent application for the use of agrin for cartilage regeneration.

Data and materials availability: All data associated with this study are present in the paper or the Supplementary Materials. Plasmids are available upon request.

Figure legends

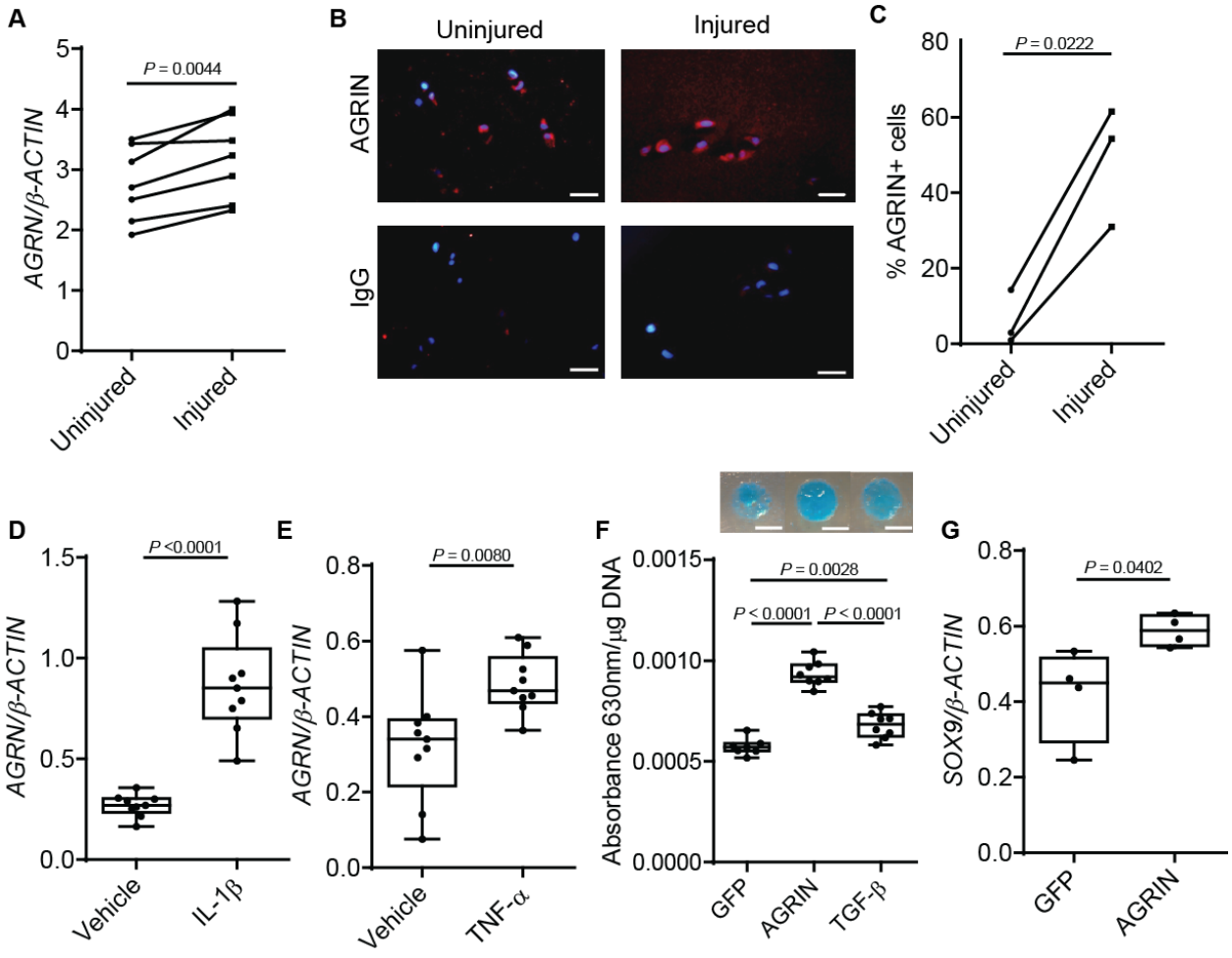

Fig. 1. Agrin is upregulated after cartilage injury, induces chondrogenesis in MSCs, and is chondrogenic in joint-resident MSCs. (**A**) RT-PCR for *AGRN* of human adult articular cartilage explants after mechanical injury or in control conditions ($n = 7$), paired t-test $P = 0.0044$. Individual values plotted. (**B**) AGRIN immunostaining (red) of human adult articular cartilage explants after mechanical injury or in control conditions; bars 50 µm, counterstained with DAPI (blue). (**C**) Quantification of AGRIN staining normalized for number of cells ($n = 3$), paired t-test $P = 0.0222$. Individual values plotted. (**D**) RT-PCR for *AGRN* in C28/I2 chondrocytes treated for 3 days with IL-1β (20 ng/ml, $n = 9$, t-test $P<0.0001$) or (**E**) TNF-α (20 ng/ml, $n = 8$, t-test $P=0.0080$). (**F**) Alcian blue staining and spectrophotometric quantitation of glycosaminoglycans in micromasses of SM-MSCs over a feeder of growth-arrested COS7 cells overexpressing AGRIN ($n = 8$), GFP

(*n* = 7), or TGF-β (*n* = 8) for 6 days, one-way ANOVA with Tukey's HSD post-hoc GFP vs AGRIN *P*<0.0001, GFP vs TGF-β *P*=0.0028, AGRIN vs TGF-β *P*<0.0001; bars 0.5mm (**G**) RT-PCR for *SOX9* of SM-MSC micromasses overexpressing AGRIN or GFP (*n* = 4), t-test *P*=0.0402. Box and whiskers plots show all values, boxes extend from the 25th to 75th percentiles, error bars span max to min values.

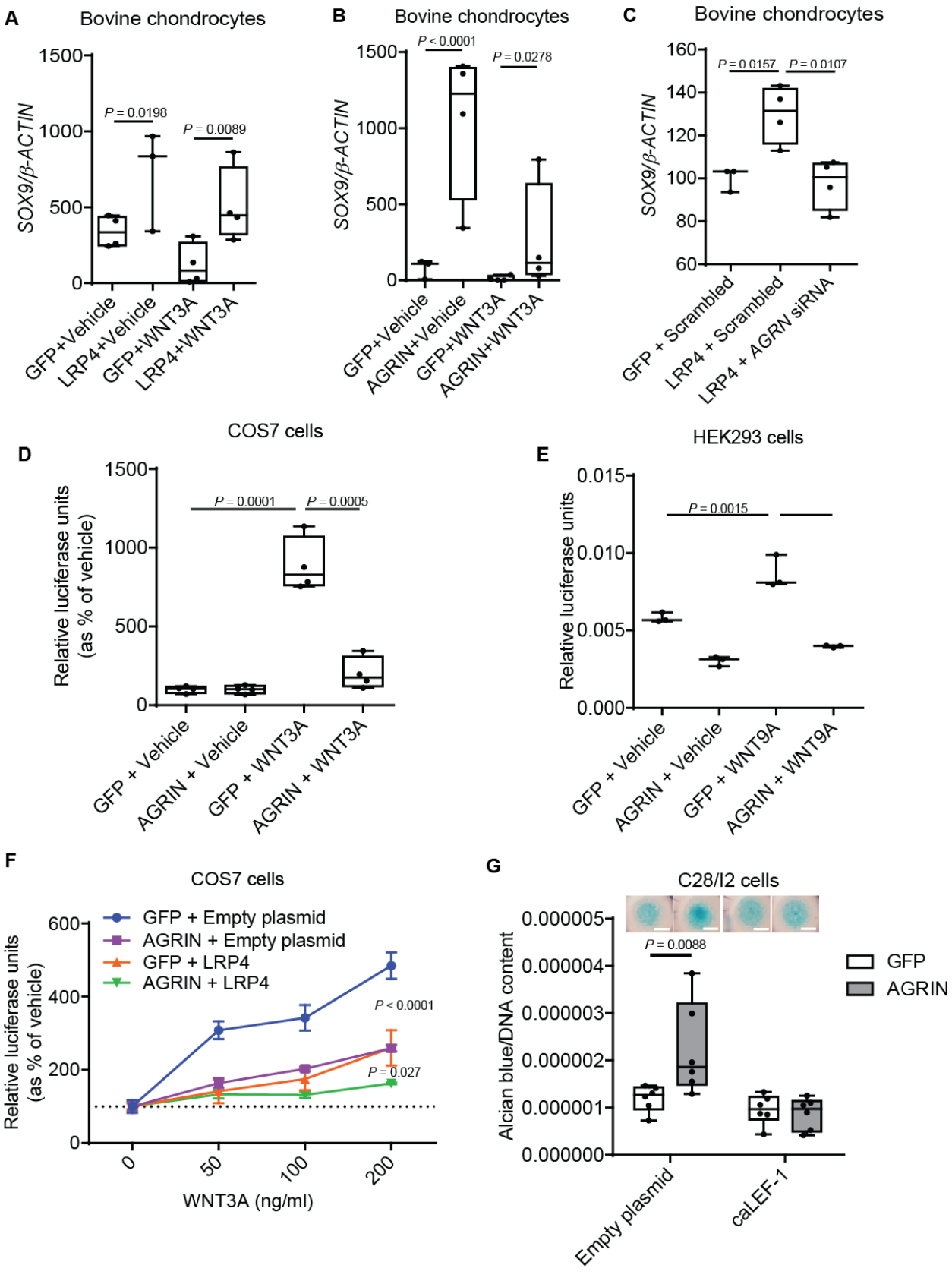
A
Bovine chondrocytes
SOX9/β-ACTIN
P = 0.0198
P = 0.0089
GFP+Vehicle
LRP4+Vehicle
GFP+WNT3A
LRP4+WNT3A
B
Bovine chondrocytes
P < 0.0001
P = 0.0278
GFP+Vehicle
AGRIN+Vehicle
GFP+WNT3A
AGRIN+WNT3A
C
Bovine chondrocytes
P = 0.0157
P = 0.0107
GFP + Scrambled
LRP4 + Scrambled
LRP4 + AGRN siRNA
D
COS7 cells
Relative luciferase units (as % of vehicle)
P = 0.0001
P = 0.0005
GFP + Vehicle
AGRIN + Vehicle
GFP + WNT3A
AGRIN + WNT3A
E
HEK293 cells
Relative luciferase units
P = 0.0015
GFP + Vehicle
AGRIN + Vehicle
GFP + WNT9A
AGRIN + WNT9A
F
COS7 cells
GFP + Empty plasmid
AGRIN + Empty plasmid
GFP + LRP4
AGRIN + LRP4
Relative luciferase units (as % of vehicle)
P < 0.0001
P = 0.027
WNT3A (ng/ml)
G
C28/I2 cells
Alcian blue/DNA content
P = 0.0088
GFP
AGRIN
Empty plasmid
caLEF-1

858

Fig. 2. Agrin/LRP4 signaling activates chondrogenesis by inhibiting WNT signaling.

(**A-C**) RT-PCR for *SOX9* of primary bovine chondrocytes transfected with (**A** and **C**) LRP4 or (**B**) AGRIN and treated with (A-B) recombinant WNT3A or (**C**) co-transfected with *AGRN* siRNA (*n* = 3, lined bars; *n* =4, square bars)); (**A**) *SOX9* levels were compared using a generalized linear model followed by pairwise comparison within each WNT3A treatment (Tukey correction), GFP+Vehicle vs LRP4+vehicle P=0.0198, GFP+WNT3A vs LRP4+WNT3A P=0.0089. (**B**) Square root transformed *SOX9* levels were compared using a generalized linear model followed by pairwise comparison within each WNT3A treatment (Tukey correction), AGRIN+Vehicle vs GFP+Vehicle P<0.0001, AGRIN+WNT3A vs GFP+WNT3A P= 0.0278; (**C**) t-test, GFP+Scrambled vs LRP4+Scrambled P=0.0157, LRP4+Scrambled vs LRP4+*AGRN* siRNA P=0.0107. (**D**) TOPFlash reporter assay in COS7 cells transduced with AGRIN or GFP and treated with recombinant WNT3A (100 ng/ml) (*n* = 4); t-test GFP vehicle vs GFP WNT3A P=0.0001, GFP WNT3A vs AGRIN WNT3A P=0.0005. (**E**) TOPFlash reporter assay in HEK293 cells transfected with AGRIN or GFP and treated with recombinant WNT9A (200 ng/ml) (*n* = 3); one way ANOVA with Tukey GFP + Vehicle vs GFP+WNT9A P=0.0015, GFP+WNT9A vs AGRIN+WNT9A p<0.0001. (**F**) TOPFlash reporter assay of COS7 cells stably expressing AGRIN or GFP and transfected with either Empty plasmid or LRP4 plasmid and treated with increasing doses of recombinant WNT3A (*n* = 4; two-way ANOVA – Tukey HSD. AGRIN vs GFP P<0.0001; AGRIN+LRP4 vs AGRIN P= 0.027. Mean values with SEM are plotted. (**G**) Alcian blue staining and quantification of C28I/2 chondrocytes in micromass culture 4 days after transfection with AGRIN or GFP with or without caLEF-1 (*n* = 4) two-way ANOVA P=0.0088; bars 0.5 mm. Box and whiskers plots show all values, boxes extend from the 25th to 75th percentiles, error bars span max to min values.

882

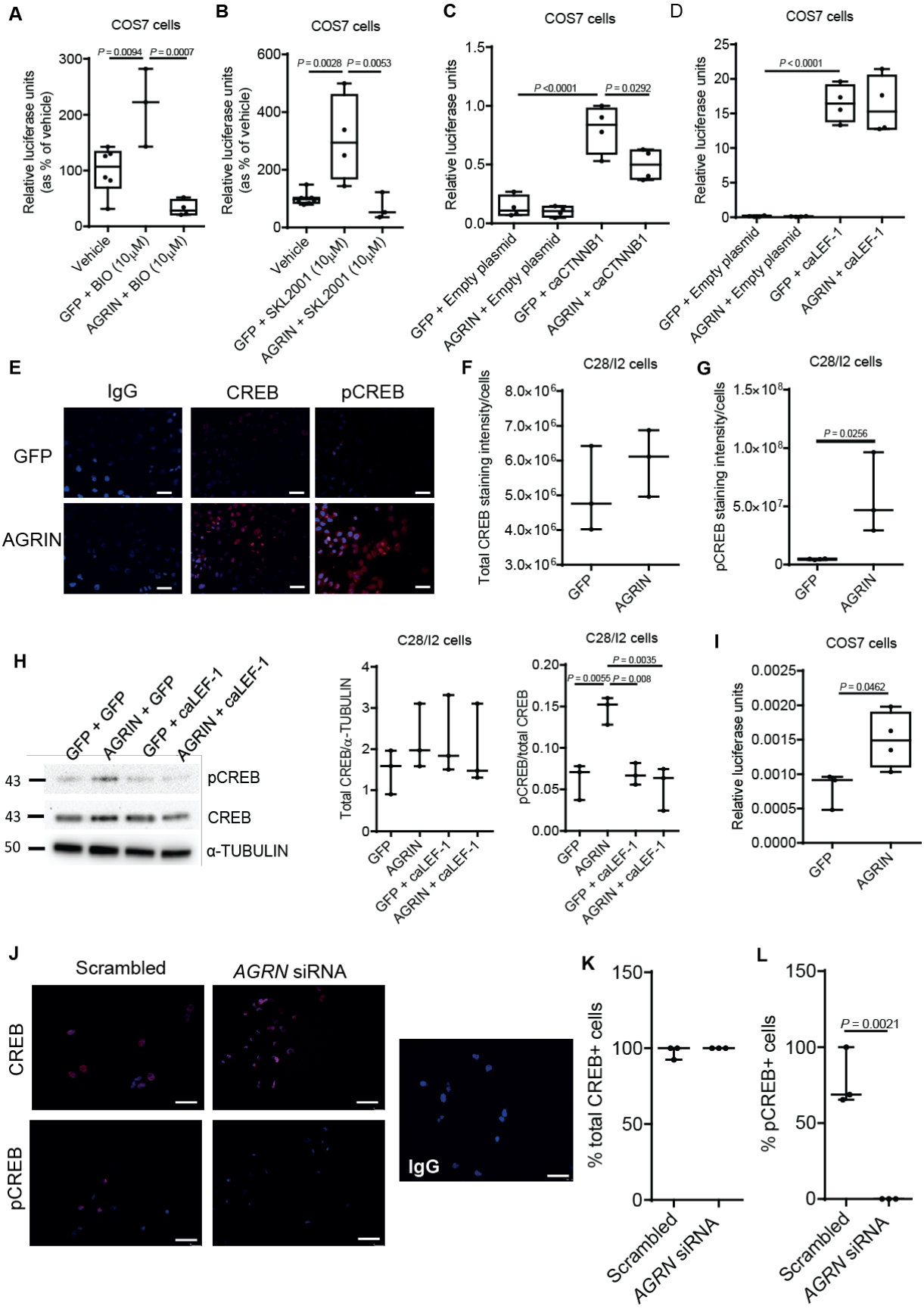
A
COS7 cells
Relative luciferase units (as % of vehicle)
P = 0.0094
P = 0.0007
Vehicle
GFP + BIO (10μM)
AGRIN + BIO (10μM)
B
COS7 cells
Relative luciferase units (as % of vehicle)
P = 0.0028
P = 0.0053
Vehicle
GFP + SKL2001 (10μM)
AGRIN + SKL2001 (10μM)
C
COS7 cells
Relative luciferase units
P < 0.0001
P = 0.0292
GFP + Empty plasmid
AGRIN + Empty plasmid
GFP + caCTNNB1
AGRIN + caCTNNB1
D
COS7 cells
Relative luciferase units
P < 0.0001
GFP + Empty plasmid
AGRIN + Empty plasmid
GFP + caLEF-1
AGRIN + caLEF-1
E
IgG
CREB
pCREB
GFP
AGRIN
F
C28/I2 cells
Total CREB staining intensity/cells
GFP
AGRIN
G
C28/I2 cells
pCREB staining intensity/cells
P = 0.0256
GFP
AGRIN
H
GFP + GFP
AGRIN + GFP
GFP + caLEF-1
AGRIN + caLEF-1
43
pCREB
43
CREB
50
α-TUBULIN
C28/I2 cells
Total CREB/α-TUBULIN
GFP
AGRIN
GFP + caLEF-1
AGRIN + caLEF-1
C28/I2 cells
pCREB/total CREB
P = 0.0035
P = 0.0055
P = 0.008
GFP
AGRIN
GFP + caLEF-1
AGRIN + caLEF-1
I
COS7 cells
Relative luciferase units
P = 0.0462
GFP
AGRIN
J
Scrambled
AGRN siRNA
CREB
pCREB
IgG
K
% total CREB+ cells
Scrambled
AGRN siRNA
L
% pCREB+ cells
P = 0.0021
Scrambled
AGRN siRNA

883

Fig. 3. Agrin inhibits canonical WNT signaling downstream of β-catenin and activates CREB-dependent transcription.

(**A**) TOPFlash reporter assay in COS7 cells transduced with AGRIN or GFP treated with BIO, (GFP+ Vehicle, *n* = 6, GFP + BIO *n* = 3, AGRIN+ BIO *n* = 4), (**B**) SKL2001, (GFP + Vehicle *n* = 8, GFP + SKL2001 *n* = 4, AGRIN + SKL2001 *n* = 3), (**C**) transfected with caCTNNB1(Δex3) (*n* = 4) or (**D**) constitutively active LEF-1 (*n* = 4); (**A** to **D**) one-way ANOVA followed by Tukey's HSD post-hoc. (**A**) Vehicle vs GFP+BIO P=0.0094, GFP+BIO vs AGRIN+BIO P=0.0007, (**B**) Vehicle vs GFP+SKL2001 P=0.0028, GFP+SKL2001 vs AGRIN+SKL2001 P=0.0053, (**C**) GFP+Empty plasmid vs AGRIN+Empty plasmid P<0.0001, GFP+caCTNNB1 vs AGRIN+caCTNNB1 P=0.0292, (**D**) GFP+Empty plasmid vs GFP+caLEF1 P<0.0001. (**E**) Immunostaining for CREB or phosphorylated CREB (pCREB) in C28/I2 cells 24 hr after transfection with AGRIN or GFP (red) with DAPI counterstain (blue). Quantification in (**F** and **G**) (*n* = 3); (**G**) t-test P=0.0256. (**H**) C28/I2 chondrocytes were cultured for 3 days in micromass, transfected as indicated, and CREB phosphorylation (p-CREB) was assessed by western blotting (*n* = 3); two-way ANOVA GFP vs AGRIN P=0.0055, AGRIN vs GFP+caLEF1 P=0.008, AGRIN vs AGRIN+caLEF1 P=0.0035. (**I**) CREB reporter assay in COS7 cells transfected with AGRIN (*n* = 4) or GFP (*n* = 3); t-test P=0.0462. (**J**) Immunostaining for CREB and phosphorylated CREB (pCREB) (red) with DAPI counterstain (blue) in C28/I2 cells 24hr after transfection with Scrambled or *AGRN* siRNA and quantification in (**K and L**) (*n* = 3); t-test P=0.0021. Box and whiskers plots show all values, boxes extend from the 25th to 75th percentiles, error bars span max to min values.

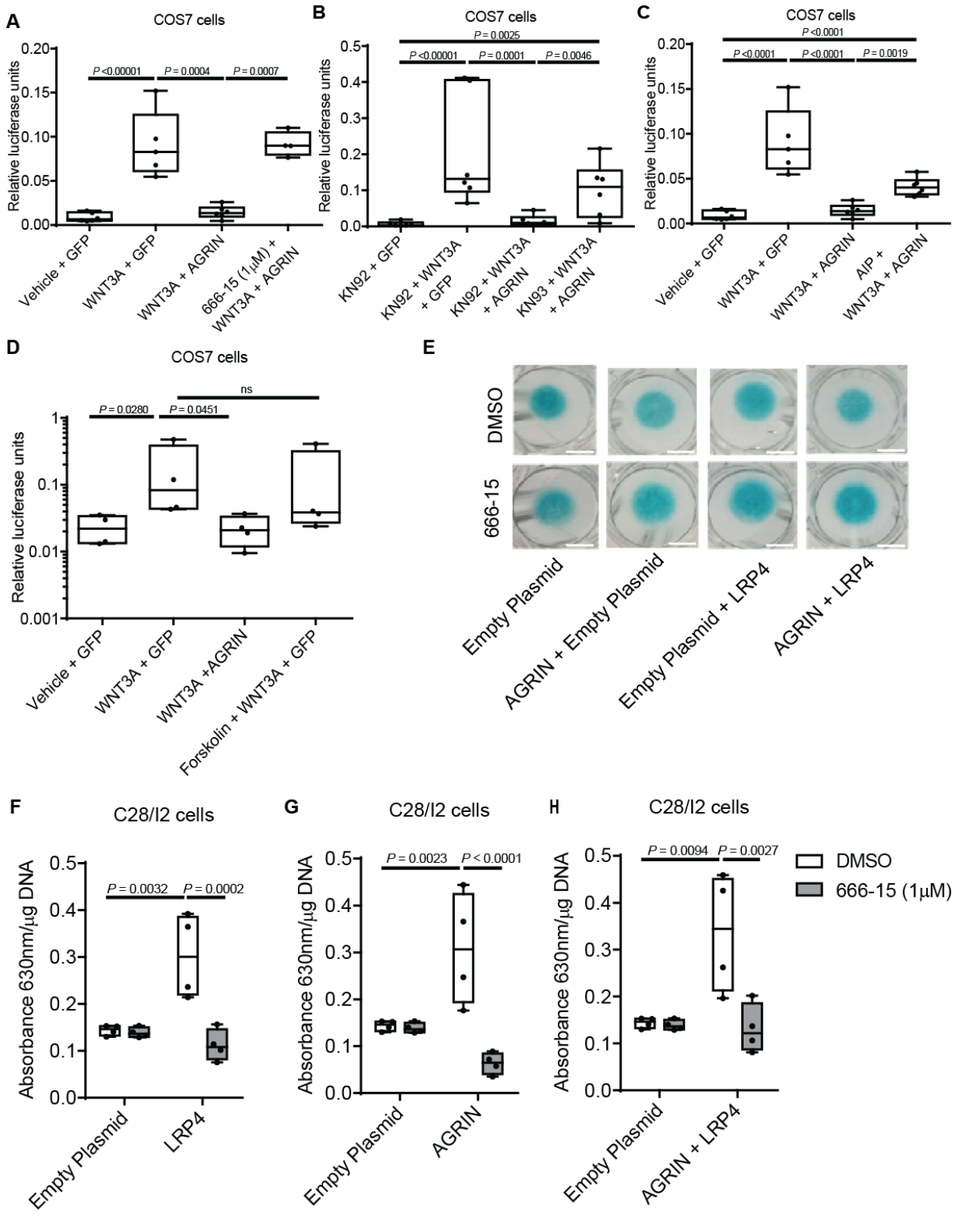
A
COS7 cells
Relative luciferase units
P <0.00001
P = 0.0004
P = 0.0007
Vehicle + GFP
WNT3A + GFP
WNT3A + AGRIN
666-15 (1μM) + WNT3A + AGRIN
B
COS7 cells
P = 0.0025
P <0.00001
P = 0.0001
P = 0.0046
KN92 + GFP
KN92 + WNT3A + GFP
KN92 + WNT3A + AGRIN
KN93 + WNT3A + AGRIN
C
COS7 cells
P <0.0001
P <0.0001
P <0.0001
P = 0.0019
Vehicle + GFP
WNT3A + GFP
WNT3A + AGRIN
AIP + WNT3A + AGRIN
D
COS7 cells
ns
P = 0.0280
P = 0.0451
Relative luciferase units
Vehicle + GFP
WNT3A + GFP
WNT3A +AGRIN
Forskolin + WNT3A + GFP
E
DMSO
666-15
Empty Plasmid
AGRIN + Empty Plasmid
Empty Plasmid + LRP4
AGRIN + LRP4
F
C28/I2 cells
Absorbance 630nm/μg DNA
P = 0.0032
P = 0.0002
Empty Plasmid
LRP4
G
C28/I2 cells
P = 0.0023
P < 0.0001
Empty Plasmid
AGRIN
H
C28/I2 cells
P = 0.0094
P = 0.0027
DMSO
666-15 (1μM)
Empty Plasmid
AGRIN + LRP4

906

Figure 4. Agrin requires CREB for its capacity to suppress WNT signaling and induce chondrogenesis.

(**A**) TOPFlash reporter assay in COS7 cells transfected with Agrin or GFP 24 hours after treatment with WNT3A in the presence or the absence of the CREB inhibitor 666-15 (n = 4). (**B** and **C**) TOPFlash reporter assay in COS7 cells transfected with AGRIN or GFP 24 hrs after WNT3A (200 ng/ml) treatment in the presence or in the absence of (**B**) the CaMKII inhibitor KN93 or its inactive control KN92 or (**C**) the CaMKII inhibitor AIP; (**A** to **C**) two-way ANOVA Tukey's HSD post-hoc, (**A**) Vehicle+GFP vs WNT3a+GFP P<0.00001, WNT3a+GFP vs WNT3a+AGRIN P=0.0004, WNT3a+AGRIN vs 666-15+WNT3a+AGRIN P=0.0007; (**B**) KN92+GFP vs KN92+WNT3A+GFP P<0.00001, KN92+WNT3A+GFP vs KN92+WNT3A+AGRIN P=0.0001, KN92+WNT3A+AGRIN vs KN93+WNT3A+AGRIN P= 0.0046, KN92+GFP vs KN93+WNT3A+AGRIN P=0.0025, (**C**) Vehicle+GFP vs WNT3A+GFP P<0.0001, Vehicle+GFP vs AIP+WNT3A+AGRIN P<0.0001, WNT3A+GFP vs WNT3A+AGRIN P<0.0001, WNT3A+AGRIN vs AIP+WNT3A+AGRIN P=0.0019. (**D**) TOPFlash reporter assay in COS7 cells transfected with either AGRIN or GFP treated with WNT3A (200 ng/ml) and/or Forskolin(10 µM); Kruskal-Wallace, overall P=0.0168. *Multiple comparison was carried out using a Dunn test,P values obtained with the Benjamini-Hochberg correction* Vehicle vs WNT3A P=0.0280, WNT3Avs WNT3A+AGRIN P=0.0451, Vehicle vs Forskolin + WNT3A +GFP. (**A** to **D** n = 4). (**E**) Representative images of Alcian blue staining of C28/I2 chondrocytes in micromass culture transfected with either empty plasmid or AGRIN and LRP4 in the presence or the absence of the CREB inhibitor 666-15; bars 0.5 mm. (**F** to **H**) Glycosaminoglycans quantification from the experiment in **E** (n = 4); log transformed values, one-way ANOVA, Tukey's HSD post-hoc, (**F**) Empty plasmid vs LRP4 P=0.0032, LRP4 vs LRP4+666-15 P=0.0002, (**G**) Empty plasmid vs

AGRIN P=0.0023, AGRIN vs AGRIN+666-15 P<0.0001, (**H**) Empty plasmid vs LRP4+AGRIN P=0.0094, AGRIN+LRP4 vs AGRIN+LRP4+666-15 P=0.0027. Box and whiskers plots show all values, boxes extend from the 25th to 75th percentiles, error bars span max to min values.

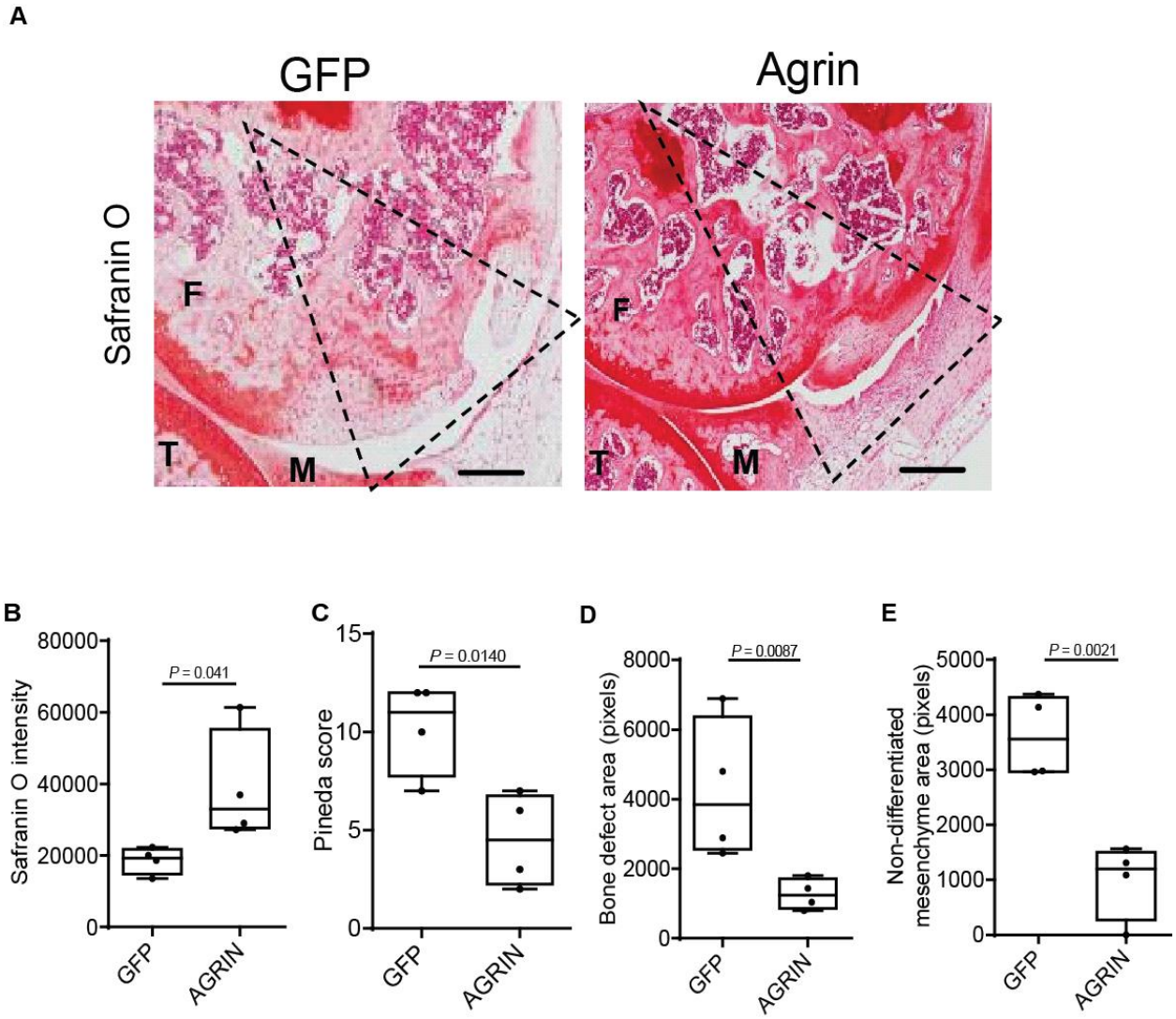

Fig. 5. Agrin supports repair morphogenesis and articular cartilage formation in vivo.

(**A**) Representative safranin O staining of the femoral condyle of C57BL/6 mice 8 weeks after the generation of an osteochondral defect filled with a collagen gel containing either AGRIN or GFP (n = 4); bars 200 µm. The dotted lines represent the approximate location of the original defect. M = meniscus; F = Femur; T = tibia (**B**) Quantification of Safranin O staining in the repair cartilage layer (n = 4). T-test after logarithmic transformation P=0.041. (**C**) Pineda score of osteochondral defect repair after 8 weeks (lower scores indicate better repair) (n = 4), Mann-Whitney U test, P=0.0140. (**D**) Histomorphometric quantification of the residual bone defect. (n = 4; Welch Two Sample t-test following log transformation; P=0.0087). (**E**) Quantification of the non-differentiated (fibroblast-like) portion of the repair mesenchyme (n = 4; Welch Two Sample t-test following log transformation; P=0.0021). Box and whiskers plots show all values, boxes extend from the 25th to 75th percentiles, error bars span max to min values.

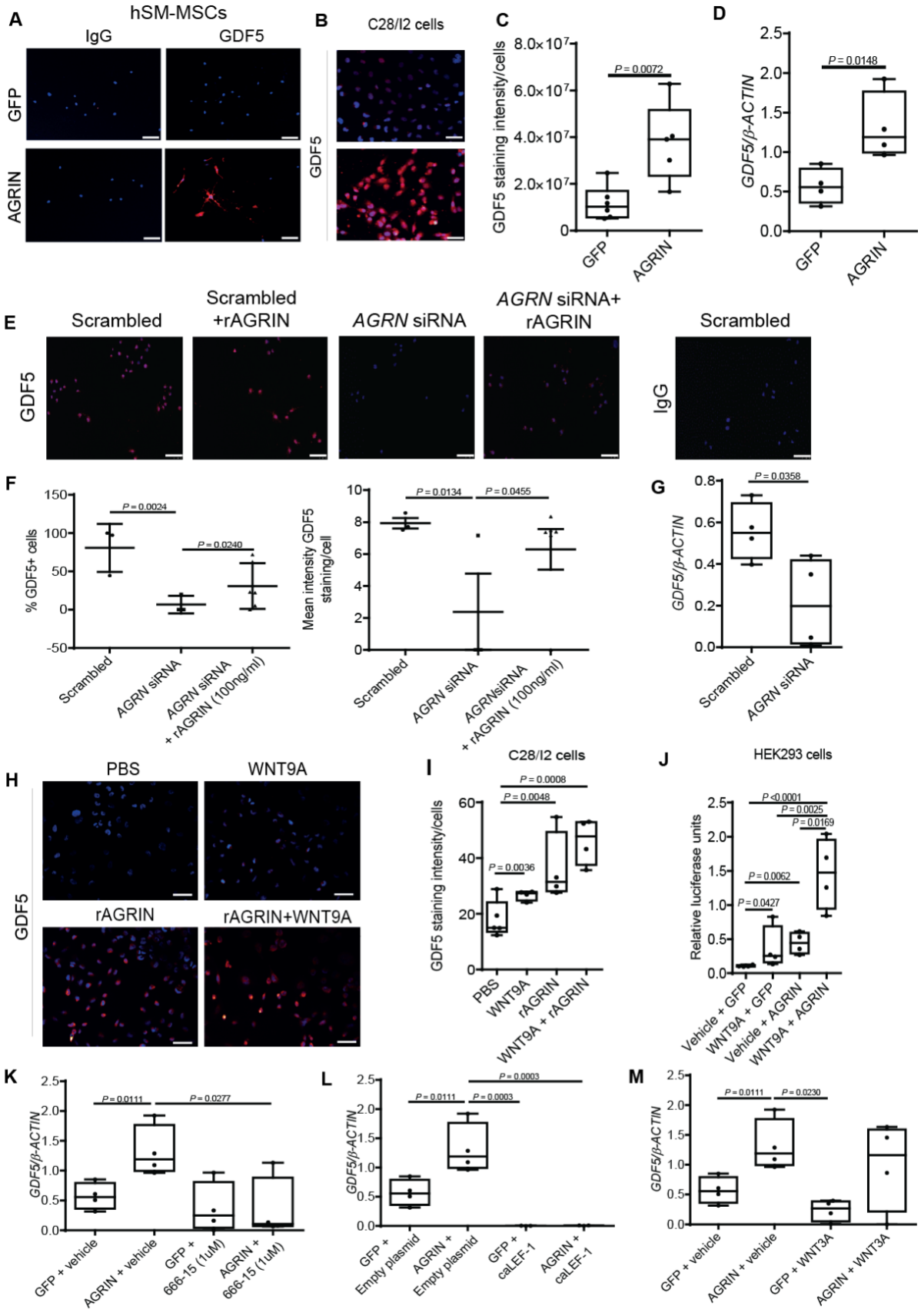
A
hSM-MSCs
IgG
GDF5
GFP
AGRIN
B
C28/I2 cells
GDF5
C
GDF5 staining intensity/cells
8.0×10^7
6.0×10^7
4.0×10^7
2.0×10^7
0
P = 0.0072
GFP
AGRIN
D
GDF5/β-ACTIN
2.5
2.0
1.5
1.0
0.5
0.0
P = 0.0148
GFP
AGRIN
E
Scrambled
Scrambled +rAGRIN
AGRN siRNA
AGRN siRNA+ rAGRIN
Scrambled
IgG
GDF5
F
% GDF5+ cells
150
100
50
0
-50
P = 0.0024
P = 0.0240
Scrambled
AGRN siRNA
AGRN siRNA + rAGRIN (100ng/ml)
Mean intensity GDF5 staining/cell
10
8
6
4
2
0
P = 0.0134
P = 0.0455
Scrambled
AGRN siRNA
AGRNsiRNA + rAGRIN (100ng/ml)
G
GDF5/β-ACTIN
0.8
0.6
0.4
0.2
0.0
P = 0.0358
Scrambled
AGRN siRNA
H
PBS
WNT9A
GDF5
rAGRIN
rAGRIN+WNT9A
I
C28/I2 cells
GDF5 staining intensity/cells
60
40
20
0
P = 0.0008
P = 0.0048
P = 0.0036
PBS
WNT9A
rAGRIN
WNT9A + rAGRIN
J
HEK293 cells
Relative luciferase units
2.5
2.0
1.5
1.0
0.5
0.0
P <0.0001
P = 0.0025
P = 0.0169
P = 0.0062
P = 0.0427
Vehicle + GFP
WNT9A + GFP
Vehicle + AGRIN
WNT9A + AGRIN
K
GDF5/β-ACTIN
2.5
2.0
1.5
1.0
0.5
0.0
P = 0.0111
P = 0.0277
GFP + vehicle
AGRIN + vehicle
GFP + 666-15 (1uM)
AGRIN + 666-15 (1uM)
L
GDF5/β-ACTIN
2.5
2.0
1.5
1.0
0.5
0.0
P = 0.0003
P = 0.0111
P = 0.0003
GFP + Empty plasmid
AGRIN + Empty plasmid
GFP + caLEF-1
AGRIN + caLEF-1
M
GDF5/β-ACTIN
2.5
2.0
1.5
1.0
0.5
0.0
P = 0.0111
P = 0.0230
GFP + vehicle
AGRIN + vehicle
GFP + WNT3A
AGRIN + WNT3A

947

Fig. 6. Agrin supports GDF5 expression in synovial membrane MSCs

(**A** and **B**) GDF5 immunocytochemistry of SM-MSCs (**A**) or C28/I2 cells (**B**) transfected with AGRIN or GFP (red) and cultured in monolayer for 24 hrs (n = 4); bars 50 µm. DAPI counterstain. (**C**) Quantification of GDF5 staining intensity in (**B**) normalized by number of cells; t-test P=0.0072. (**D**) RT-PCR for *GDF5* in C28/I2 cells transfected with AGRIN or GFP and cultured for 3 days in micromass (n = 4); t-test P=0.0148. (**E**) GDF5 immunocytochemistry (red) counterstained with DAPI (blue) of C28/I2 cells cultured in monolayer for 24 hrs following transfection with Scrambled or *AGRN* siRNA in the presence or absence of rAGRIN; bars 50 µm. (**F**) Quantification of % GDF5+ cells from (**E**) Scrambled n = 3; *AGRN* siRNA n = 3; *AGRN* siRNA+rAGRIN n = 6) one-way ANOVA Scrambled vs *AGRN* siRNA P=0.0024, *AGRN* siRNA vs *AGRN* siRNA+rAGRIN P=0.024; and mean intensity per cell, one-way ANOVA using generalized linear model followed by pairwise comparison within each Scrambled vs *AGRN* siRNA P=0.0134, *AGRN* siRNA vs *AGRN* siRNA+rAGRIN P=0.0455. (**G**) RT-PCR for *GDF5* in C28/I2 cells transfected with Scrambled or *AGRN* siRNA cultured for 3 days in micromass (n = 4); t-test P= 0.0358. (**H**) Immunostaining for GDF5 in C28/I2 chondrocytes treated with recombinant AGRIN (300 ng/ml) and/or WNT9A (200 ng/ml) for 24 hrs; bars 50 µm; and (**I**) quantification (n = 4); after reciprocal transformation values were compared by one-way ANOVA with Tukey HSD post-hoc for multiple comparisons P=0.0008; PBS vs WNT9A P=0.0036, PBS vs rAGRIN P=0.0048, PBS vs WNT9A+AGRIN P=0.0008. (**J**) CREB reporter assay in HEK293 cells treated with recombinant AGRIN (300 ng/ml)and/or WNT9A (200 ng/ml) (n = 4); one-way ANOVA with Tukey test for multiple comparisons on log transformed values P=Vehicle+GFP vs WNT9A+GFP P=0.0427630, Vehicle+GFP vs Vehicle+AGRIN P=0.0063, Vehicle+GFP vs WNT9A+AGRIN $P<0.0001$, Vehicle+AGRIN vs WNT9A+AGRIN P=0.0169, WNT9A+GFP vs

WNT9A+AGRIN P=0.0025. (**K** to **M**) RT-PCR for *GDF5* mRNA in C28/I2 cells transfected with AGRIN or GFP plasmids, cultured in micromass for 4 days and treated in the presence of (**K**) 666-15 (1 μM) or vehicle or (**L**) co-transfected with caLEF1 plasmid or (**M**) recombinant WNT3A (200 ng/ml) (n = 4); one-way ANOVA with Tukey's HSD post-hoc (**K**) GFP vs AGRIN P=0.0111, AGRIN+vehicle vs AGRIN666-15 P=0.0277, (**L**) GFP vs AGRIN P=0.0111, AGRIN vs GFP+caLEF1 P=0.0003, AGRIN vs AGRIN+caLEF1 P=0.00033, (M) AGRIN+vehicle vs GFP+WNT3A P=0.0230. Box and whiskers plots show all values, boxes extend from the 25th to 75th percentiles, error bars span max to min values.

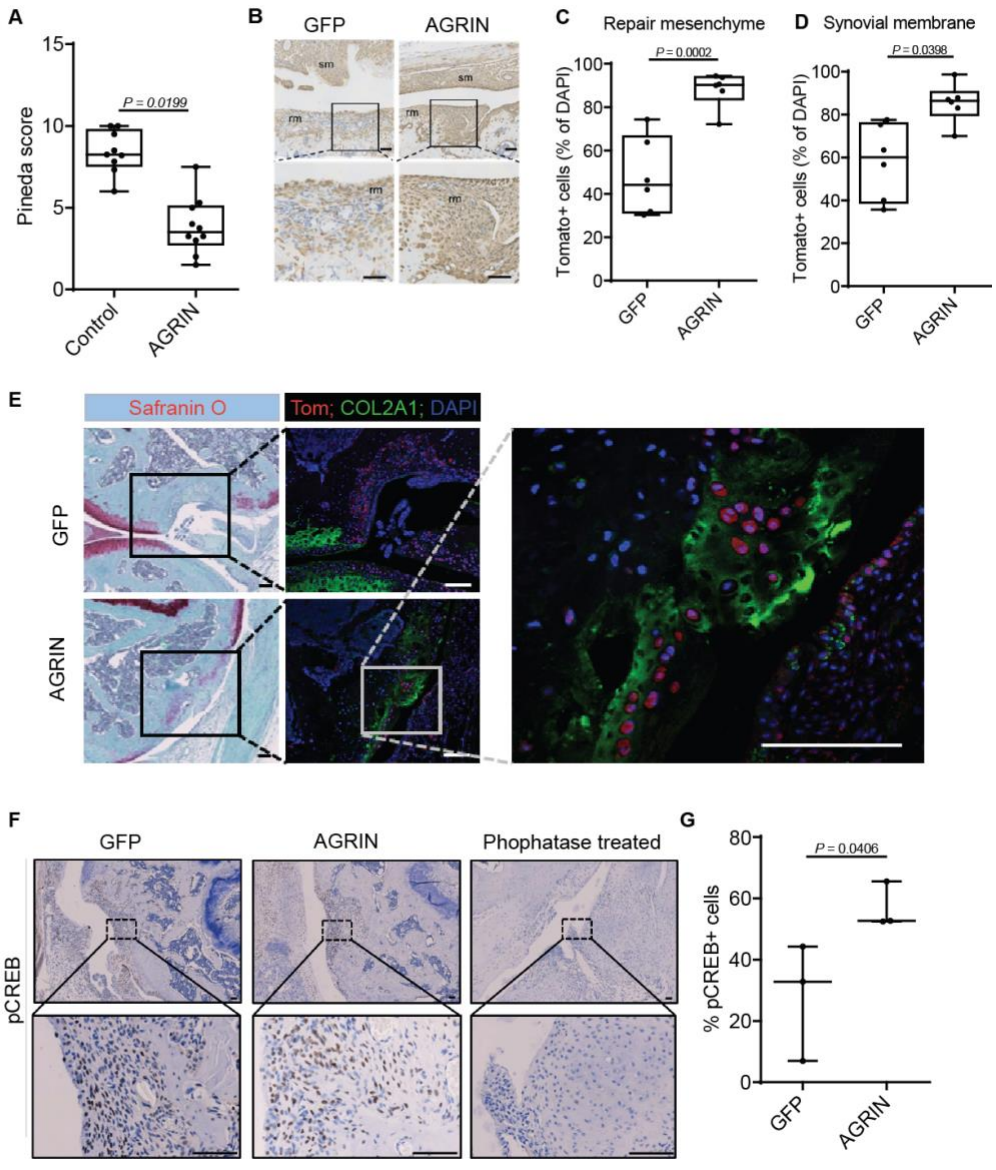

980

981 **Fig. 7. Agrin-induced joint surface repair is associated with increased recruitment of Gdf5-**

982 **lineage joint stem cells and CREB phosphorylation in the repair mesenchyme.**

983 (**A**) Pineda score of *Gdf5*:Tom transgenic mice 8 weeks after the generation of an osteochondral

984 defect filled with either agrin or GFP (n = 9 GFP, n = 10 AGRIN; Mann-Whitney U test;

985 P=0.01994). (**B**) Immunohistochemistry for Tomato in the defect of *Gdf5*:Tom transgenic mice 3

weeks after the generation of an osteochondral defect filled with a collagen gel containing either AGRIN or GFP; sm=synovial membrane; rm=repair mesenchyme (n = 6). Boxed region shown at higher magnification below; bars 50 µm. (**C**) Quantification of Tom+ cells in the repair mesenchyme and (**D**) in the synovial membrane; t-test (**C**) P=0.0002, (**D**) P=0.0398. Box and whiskers plots show all values, boxes extend from the 25th to 75th percentiles, error bars span max to min values. (**E**) Safranin O (left panels) and immunofluorescence (right) for Tomato (red) and Collagen type 2 (green) 8 weeks post-surgery, counter stained for DAPI (blue). Boxed region shown at higher magnification below; bars 100 µm. Immunohistochemistry (**F**) and quantification (**G**) of phospho-CREB (pCREB) in the repair mesenchyme of *Gdf5*;Tom mice treated with AGRIN or control, 3 weeks after the generation of an osteochondral defect (n = 3); phosphatase treatment was used as staining control; (**F**) Welch two sample t-test of squared values P=0.04058; bars 100 µm. Mean values with SEM are plotted.

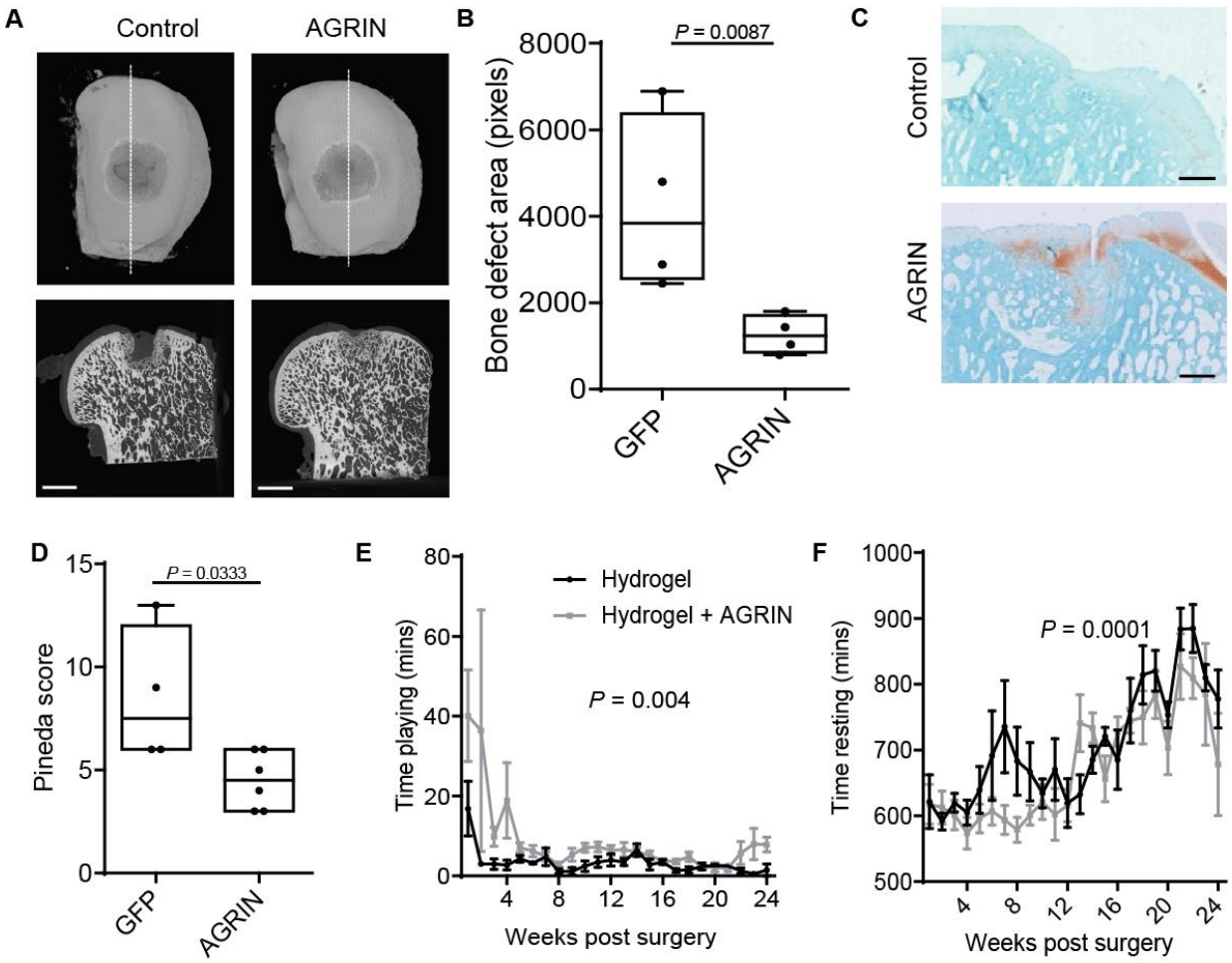
A
Control
AGRIN
B
P = 0.0087
Bone defect area (pixels)
8000
6000
4000
2000
0
GFP
AGRIN
C
Control
AGRIN
D
P = 0.0333
Pineda score
15
10
5
0
GFP
AGRIN
E
Hydrogel
Hydrogel + AGRIN
P = 0.004
Time playing (mins)
80
60
40
20
0
4
8
12
16
20
24
Weeks post surgery
F
P = 0.0001
Time resting (mins)
1000
900
800
700
600
500
4
8
12
16
20
24
Weeks post surgery

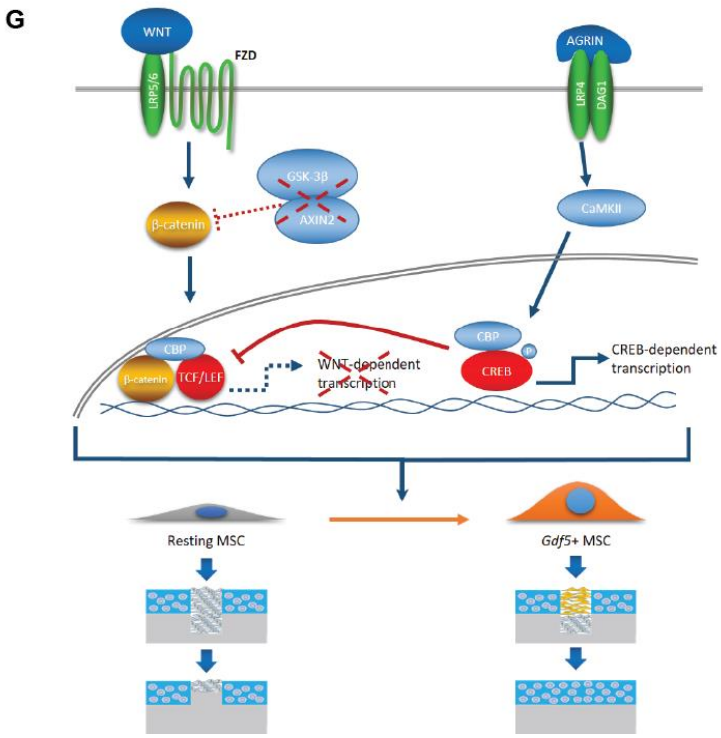
G
WNT
FZD
LRP5/6
AGRIN
LRP4
DAG1
GSK 3β
β-catenin
AXIN2
CaMKII
CBP
β-catenin
TCF/LEF
WNT-dependent transcription
CBP
CREB
CREB-dependent transcription
Resting MSC
Gdf5+ MSC

998

Figure 8. A single administration of agrin in critical size joint surface defects in sheep regenerates the articular cartilage.

Sheep underwent the generation of an osteochondral defect that was filled with a collagen gel containing AGRIN or GFP and killed after 6 months (n = 6). (**A**) Representative µCT images of defects at 6-month time-point (n = 6; scale bar 5mm) and (**B**) quantification of the residual non-calcified defect area (n = 6 control and n = 5 Agrin; Welch t-test after log transformation, P=0.0134). (**C**) Safranin O staining of the joint surface defect area, bars 200 µm. (**D**) Pineda score (n = 4 controls and n = 6 AGRIN; Mann-Whitney U test P=0.0333. (**E**) Time spent playing (two-way ANOVA, Treatment P=0.00495) and (**F**) time spent resting (two-way ANOVA, Treatment P=0.00043). (**G**) AGRIN promotes the morphogenesis of the repair mesenchyme at the site of cartilage injury. This process involves the activation of CREB-dependent upregulation of *Gdf5* and suppression of WNT signaling downstream of β-catenin.

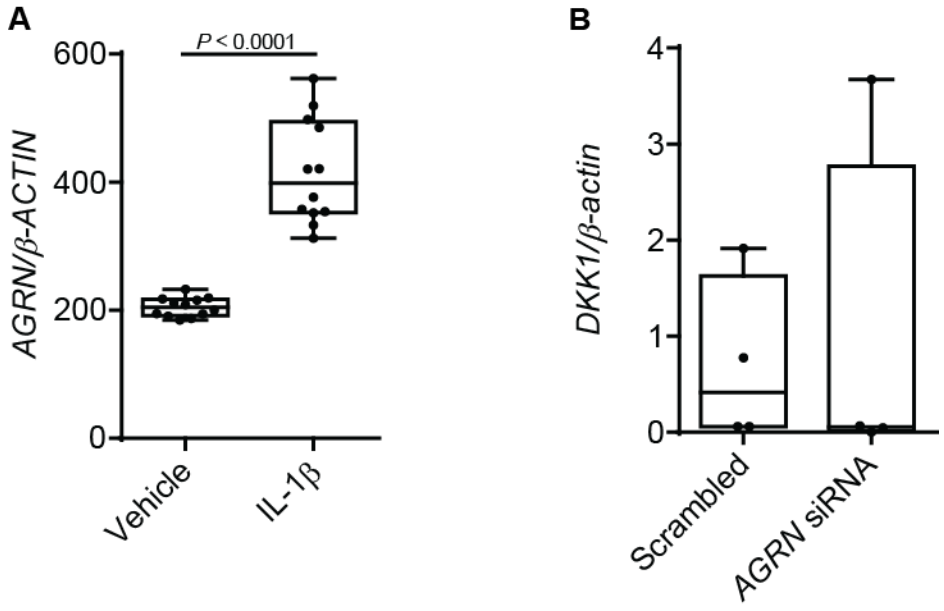

Supplementary figure 1. (**A**) Microarray human chondrocytes – (mined from GEO accession GSE75181[30]), *P*< 0.0001 (*n* = 12). (**B**) RT-PCR for *DKK1*in C28/I2 cells transfected with Scrambled or *AGRN* siRNA cultured for 3 days in micromass (*n* = 4).

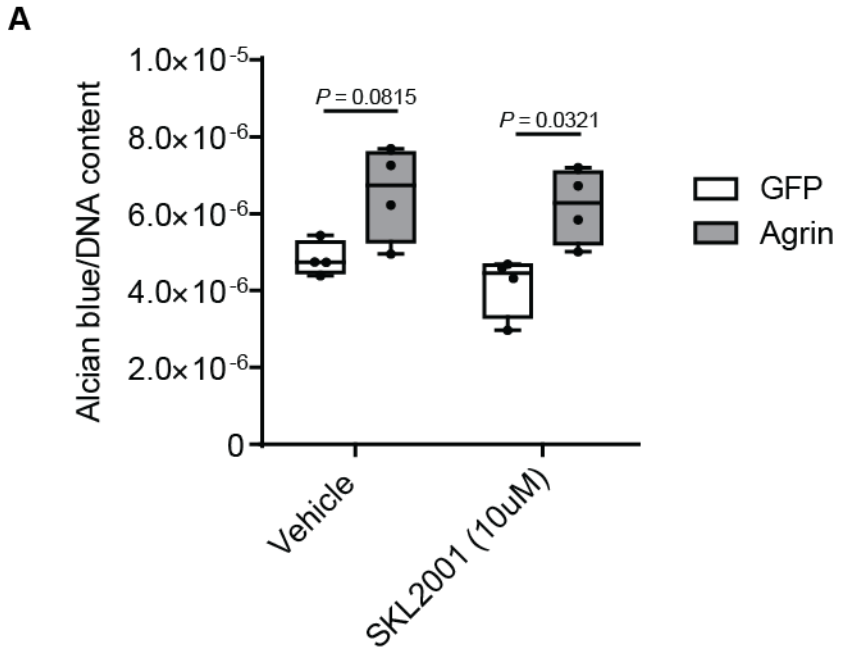

Supplementary figure 2. Alcian blue staining and quantification of C28I/2 chondrocytes in micromass culture 4 days after transfection with GFP or AGRIN with or without SKL2001 (*n* = 4), two-way ANOVA P=0.0013, GFP + Vehicle vs AGRIN + Vehicle *P*= 0.0815, GFP + SKL2001 vs Agrin + SKL2001 *P*=0.0321.

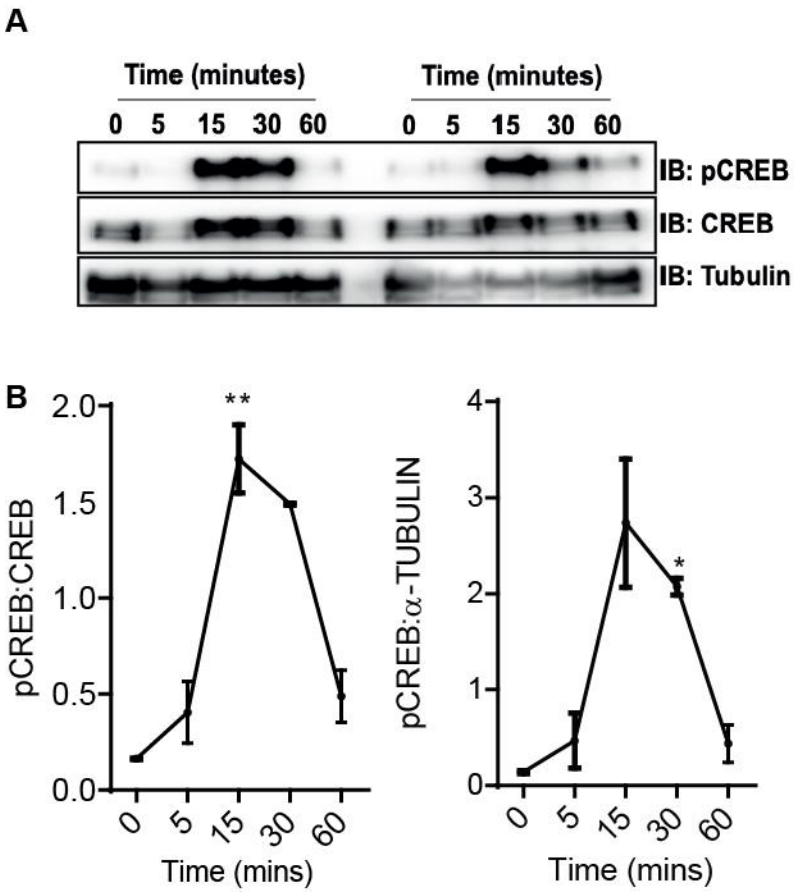

Supplementary figure 3. (**A**) Temporal analysis by western blot of pCREB in C28/I2 cells treated with 100 ng/ml rAgrin normalized to (**B**) CREB and tubulin (one-way ANOVA followed by Dunnets multiple comparison test) (n = 2).

A

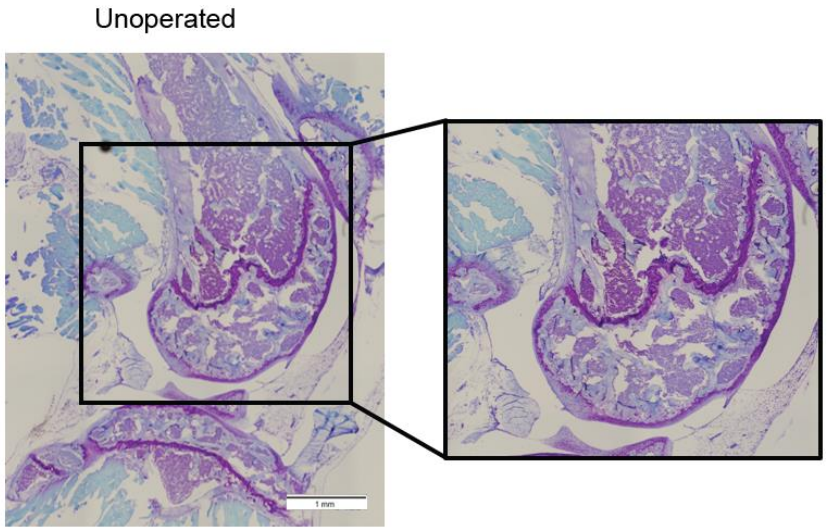

B

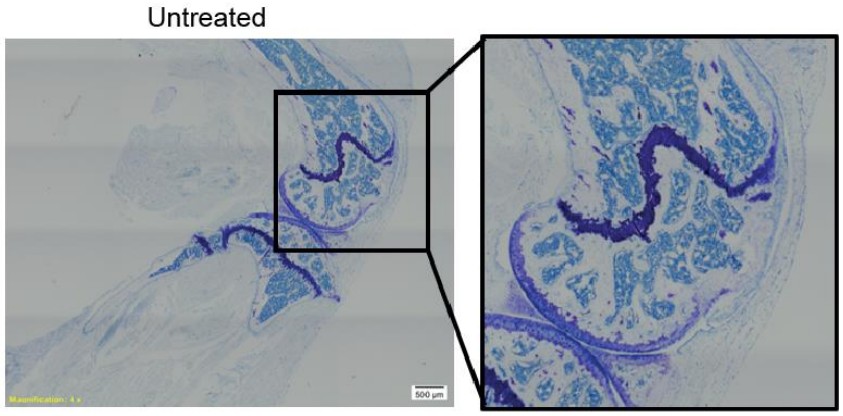

C

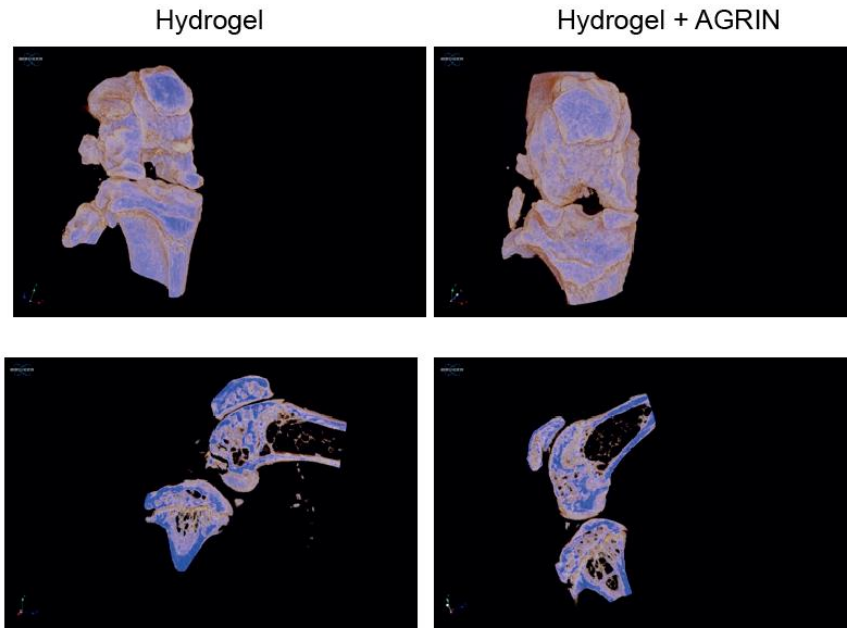

1028

Supplementary figure 4. (**A**) Unoperated joint of a mouse stained with Toludine blue. (**B**) Untreated subchondral defect in mice 8 weeks post-surgery stained with toluidine blue. (**C**) MicroCT of *Gdf*5-Cre;Tom mice 8 weeks post-surgery.

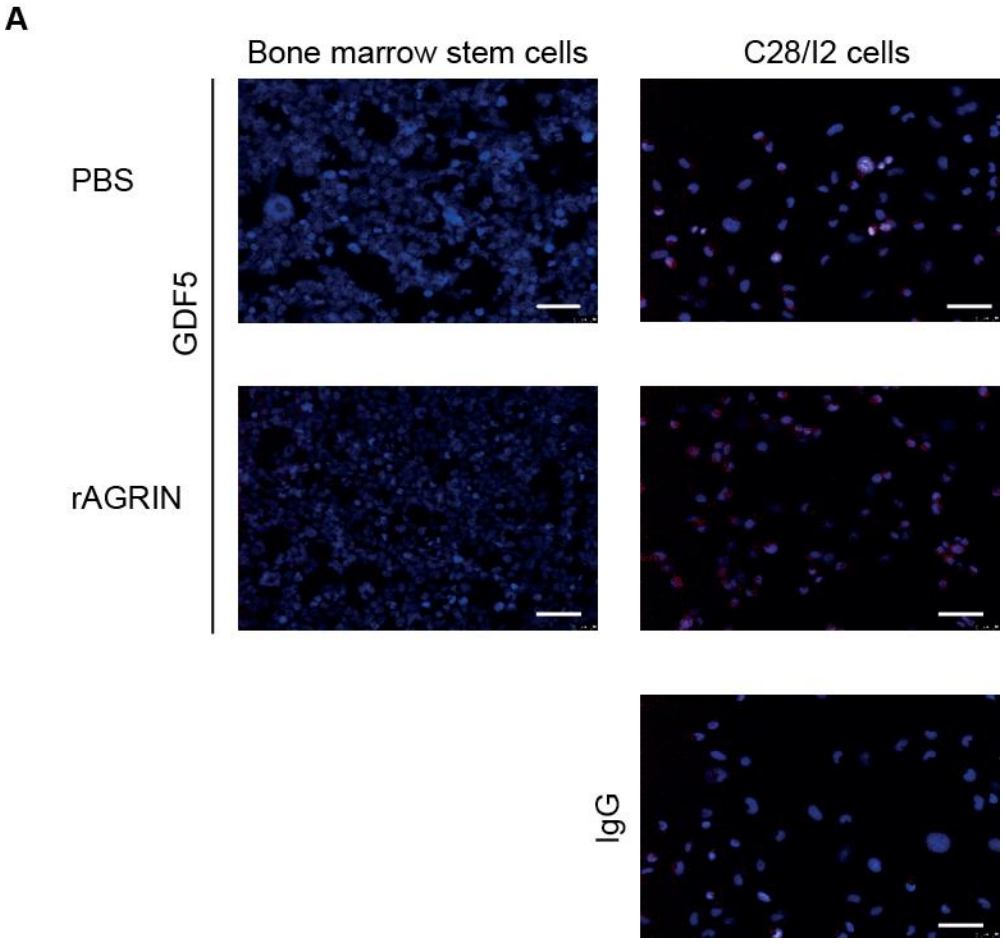

Supplementary figure 5. Immunofluorescence for GDF5 in murine bone marrow derived stem cells treated with rAgrin (100 ng/ml) compared to C28/I2 chondrocytes as positive control; bars 50µm (n = 4).

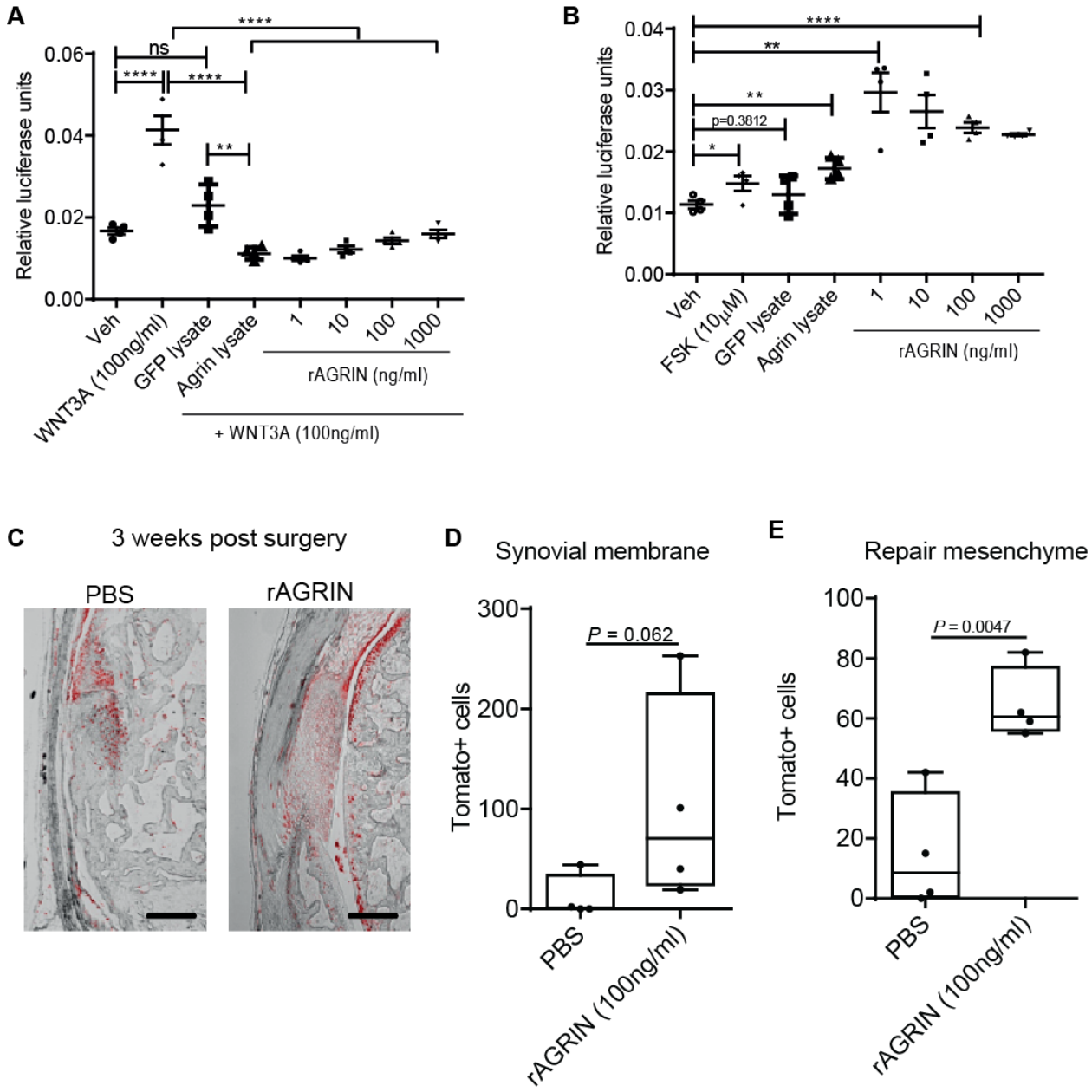

1036

1037 **Supplementary figure 6.** (**A**) TOPFlash reporter assay of HEK293 cells cultured in the presence

1038 of COS7-AGRIN or COS7-GFP cell lysate (used at ratio equal to in vivo) and compared to

1039 increasing doses of recombinant Agrin (rAgrin) in the presence of WNT3A (*n* = 4). (**B**) CREB

1040 reporter assay of HEK293 cells cultured in the presence of COS7-AGRIN or COS7-GFP cell

lysate (used at ratio equal to in vivo) and compared to increasing doses of recombinant AGRIN (rAGRIN), forskolin was used as a positive control (n = 4); (**A** and **B**) one-way ANOVA, *=p<0.05, **=p<0.01,***=p<0.001, ****=p<0.0001. (**C**) Immunofluorescence for Tomato in the defect of *Gdf5*:Tom transgenic mice 3 weeks after the generation of a joint surface defect filled with a collagen gel containing either rAGRIN (100 ng/ml) or PBS; bars 200 µm. Quantification of the number of Tom+ cells in (**D**) the synovial membrane and (**E**) repair mesenchyme in the defect site.

Supplementary table 1. Ages of operated sheep. COS7-GFP treated group mean age 2.9 years ± 0.45 (SD); COS7-AGRIN treated group mean age 2.95 years ± 0.40 (SD).

Treatment group	Age	Exclusion
COS7-GFP	2.6	
COS7-GFP	2.5	
COS7-GFP	3.3	
COS7-GFP	3.6	Osteomyelitis in the forelimb, CT analysis only
COS7-GFP	2.6	Cyst, CT analysis only
COS7-GFP	2.8	
COS7-AGRIN	3.4	
COS7-AGRIN	2.5	
COS7-AGRIN	2.5	
COS7-AGRIN	2.8	
COS7-AGRIN	3.3	
COS7-AGRIN	3.2	

Supplementary table 2. Antibody supplier and usage information.

Antibodies	**Species**	**Code**	**Supplier**	**Western Blotting**	**Immunofluorescence**
AGRIN	Rabbit	H300	Santa Cruz Biotechnology		1:100
CREB	Rabbit	9197	Cell Signaling	1:1000	1:800
pCREB	Rabbit	9198	Cell signaling	1:1000	1:800
GDF5	Rabbit	93855	Abcam		1:1000
IgG	Rabbit	37415	Abcam		1:100-1:800
AlexaFluro555	Goat	150078	ThermoFisher		1:300
α-TUBULIN	Mouse	T5168	Sigma	1:5000	
COL2A1	Rabbit	Ab21291	Abcam		1:100
Tomato	Goat	Ab0081	Sicgen		1:100
Tomato	Rabbit	600-401-379	Rockland		1:600

Supplementary table 3. Recombinant proteins and reagents supplier and usage information.

Recombinant	Concentration	Resuspended in	Code	Supplier
IL-1β	20 ng/ml	0.1% BSA in PBS	201-LB	R&D systems
TNF-α	20 ng/ml	0.1% BSA in PBS	210-TA	R&D systems
WNT3A	50-200 ng/ml	0.1% BSA in PBS	5036-WN	R&D systems
Wnt-9A	200 ng/ml	0.1% BSA in PBS	8148-WN	R&D systems
SKL2001	10 µM	DMSO	681667	Calbiochem
BIO	10 µM	DMSO	3194	Tocris
MeBIO	10 µM	DMSO	3873	Tocris
Forskolin	10 µM	DMSO	F6886	Sigma
666-15	1 µM	DMSO	5661	Tocris
KN92	10 µM	DMSO	4130	Tocris
KN93	10 µM	DMSO	1278	Tocris
AIP	5 µM	DMSO	5959	R&D systems

Supplementary table 4. Primer and siRNA sequences

	Sense	Antisense	Amplicon (bps)
hβ-*ACTIN*	TGACGGGGTCACCCACACTGTGCCCATCTA	CTAGAAGCATTTGCGGTGGACGATGGAGG	661
h*AGRN*	CCTGACCCTCAGCTGGCCCT	AGATACCCAGGCAGGCGGCA	136
h*DKK*	ATTCCAACGCTATCAAGAAC	CCAAGGTGCTATGATCATTACC	384
h*GDF5*	AGGCAACAGCAGCGTGAAGT	GGTCATCTTGCCCTTTGTCAA	77
h*SOX9*	GAACGCACATCAAGACGGAG	TCTCGTTGATTTCGCTGCTC	631
bβ-*ACTIN*	AGGAGTCGGTTGGATCGAGCA	GGGAAGGCAAAGGACTTCCTGTAAC	136
b*SOX9*	ACTCTGGGCAAGCTCTGGAGACT	GGCGCGGCTGGTACTTGTAGTCC	121
h*AGRN* siRNA	CCUUUGUCGAGUACCUCAACGCUGU	ACAGCGUUGAGGUACUCGACAAAGG	

A Stealth RNAi negative control duplex of low GC content was used as a negative control (Invitrogen). h:human, b:bovine.

R script for download and statistical analysis of microarray data from Comblain et al. (30)

```
# Version info: R 3.2.3, Biobase 2.30.0, GEOquery 2.40.0, limma 3.26.8
# R scripts generated  Wed Sep 4 06:31:58 EDT 2019

########################################################################
#   Differential expression analysis with limma
library(Biobase)
library(GEOquery)
library(limma)

# load series and platform data from GEO

gset <- getGEO("GSE75181", GSEMatrix =TRUE, AnnotGPL=TRUE)
if (length(gset) > 1) idx <- grep("GPL10558", attr(gset, "names")) else idx <- 1
gset <- gset[[idx]]
```

```
1078  # make proper column names to match toptable
1079  fvarLabels(gset) <- make.names(fvarLabels(gset))
1080
1081  # group names for all samples
1082  gsms <- "000000000000XXXXXXXXXXXX111111111111XXXXXXXXXXXX"
1083  sml <- c()
1084  for (i in 1:nchar(gsms)) { sml[i] <- substr(gsms,i,i) }
1085
1086  # eliminate samples marked as "X"
1087  sel <- which(sml != "X")
1088  sml <- sml[sel]
1089  gset <- gset[ ,sel]
1090
1091  # log2 transform
1092  ex <- exprs(gset)
1093  qx <- as.numeric(quantile(ex, c(0., 0.25, 0.5, 0.75, 0.99, 1.0), na.rm=T))
```

```
1094  LogC <- (qx[5] > 100) ||
1095            (qx[6]-qx[1] > 50 && qx[2] > 0) ||
1096            (qx[2] > 0 && qx[2] < 1 && qx[4] > 1 && qx[4] < 2)
1097  if (LogC) { ex[which(ex <= 0)] <- NaN
1098    exprs(gset) <- log2(ex) }
1099
1100  # set up the data and proceed with analysis
1101  sml <- paste("G", sml, sep="")    # set group names
1102  fl <- as.factor(sml)
1103  gset$description <- fl
1104  design <- model.matrix(~ description + 0, gset)
1105  colnames(design) <- levels(fl)
1106  fit <- lmFit(gset, design)
1107  cont.matrix <- makeContrasts(G1-G0, levels=design)
1108  fit2 <- contrasts.fit(fit, cont.matrix)
1109  fit2 <- eBayes(fit2, 0.01)
```

```
tT <- topTable(fit2, adjust="fdr", sort.by="B", number=250)

tT <- subset(tT, select=c("ID","adj.P.Val","P.Value","t","B","logFC","Gene.symbol","Gene.title"))
write.table(tT, file=stdout(), row.names=F, sep="\t")


################################################################
#   Boxplot for selected GEO samples
library(Biobase)
library(GEOquery)

# load series and platform data from GEO

gset <- getGEO("GSE75181", GSEMatrix =TRUE, getGPL=FALSE)
if (length(gset) > 1) idx <- grep("GPL10558", attr(gset, "names")) else idx <- 1
```

```
1126 gset <- gset[[idx]]
1127
1128 # group names for all samples in a series
1129 gsms <- "000000000000XXXXXXXXXXXX111111111111XXXXXXXXXXXX"
1130 sml <- c()
1131 for (i in 1:nchar(gsms)) { sml[i] <- substr(gsms,i,i) }
1132 sml <- paste("G", sml, sep="")  set group names
1133
1134 # eliminate samples marked as "X"
1135 sel <- which(sml != "X")
1136 sml <- sml[sel]
1137 gset <- gset[ ,sel]
1138
1139 # order samples by group
1140 ex <- exprs(gset)[ , order(sml)]
1141 sml <- sml[order(sml)]
```

```
fl <- as.factor(sml)
labels <- c("Control","IL-1")

# set parameters and draw the plot
palette(c("#dfeaf4","#f4dfdf", "#AABBCC"))
dev.new(width=4+dim(gset)[[2]]/5, height=6)
par(mar=c(2+round(max(nchar(sampleNames(gset)))/2),4,2,1))
title <- paste ("GSE75181", '/', annotation(gset), " selected samples", sep ='')
boxplot(ex, boxwex=0.6, notch=T, main=title, outline=FALSE, las=2, col=fl)
legend("topleft", labels, fill=palette(), bty="n")
```